Bioactive Materials 25 (2023) 42–60

Contents lists available at ScienceDirect

Bioactive Materials

journal homepage: www.keaipublishing.com/en/journals/bioactive-materials

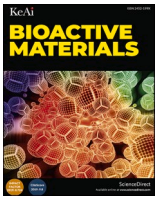

Nanofiber matrix formulations for the delivery of Exendin-4 for tendon regeneration: *In vitro* and *in vivo* assessment

Sama Abdulmalik [a,b], Jack Gallo [a,d], Jonathan Nip [a,b], Sara Katebifar [a,b], Michael Arul [a], Amir Lebaschi [a], Lucas N. Munch [a], Jenna M. Bartly [e], Shilpa Choudhary [a], Ivo Kalajzic [f], Yeshavanth Kumar Banasavadi-Siddegowdae [g], Syam P. Nukavarapu [a,b,c], Sangamesh G. Kumbar [a,b,c,*]

[a] *Department of Orthopedic Surgery, University of Connecticut Health, Farmington, CT, USA*
[b] *Department of Biomedical Engineering, University of Connecticut, Storrs, CT, USA*
[c] *Department of Materials Science and Engineering, University of Connecticut, Storrs, CT, USA*
[d] *Department of Physiology and Neurobiology, University of Connecticut, Storrs, CT, USA*
[e] *Department of Immunology, Center on Aging, University of Connecticut Health, Farmington, CT, USA*
[f] *Department of Reconstructive Sciences, University of Connecticut Health, Farmington, CT, USA*
[g] *Surgical Neurology Branch, National Institute of Neurological Disorders and Stroke, National Institutes of Health, Bethesda, MD, USA*

ARTICLE INFO

Keywords:
Nanofiber matrix formulation
Protein delivery
Soft tissue regeneration
Halloysite nanotubes

ABSTRACT

Tendon and ligament injuries are the most common musculoskeletal injuries, which not only impact the quality of life but result in a massive economic burden. Surgical interventions for tendon/ligament injuries utilize biological and/or engineered grafts to reconstruct damaged tissue, but these have limitations. Engineered matrices confer superior physicochemical properties over biological grafts but lack desirable bioactivity to promote tissue healing. While incorporating drugs can enhance bioactivity, large matrix surface areas and hydrophobicity can lead to uncontrolled burst release and/or incomplete release due to binding. To overcome these limitations, we evaluated the delivery of a peptide growth factor (exendin-4; Ex-4) using an enhanced nanofiber matrix in a tendon injury model. To overcome drug surface binding due to matrix hydrophobicity of poly (caprolactone) (PCL)—which would be expected to enhance cell-material interactions—we blended PCL and cellulose acetate (CA) and electrospun nanofiber matrices with fiber diameters ranging from 600 to 1000 nm. To avoid burst release and protect the drug, we encapsulated Ex-4 in the open lumen of halloysite nanotubes (HNTs), sealed the HNT tube endings with a polymer blend, and mixed Ex-4-loaded HNTs into the polymer mixture before electrospinning. This reduced burst release from ~75% to ~40%, but did not alter matrix morphology, fiber diameter, or tensile properties. We evaluated the bioactivity of the Ex-4 nanofiber formulation by culturing human mesenchymal stem cells (hMSCs) on matrix surfaces for 21 days and measuring tenogenic differentiation, compared with nanofiber matrices in basal media alone. Strikingly, we observed that Ex-4 nanofiber matrices accelerated the hMSC proliferation rate and elevated levels of sulfated glycosaminoglycan, tendon-related genes (Scx, Mkx, and Tnmd), and ECM-related genes (Col-I, Col-III, and Dcn), compared to control. We then assessed the safety and efficacy of Ex-4 nanofiber matrices in a full-thickness rat Achilles tendon defect with histology, marker expression, functional walking track analysis, and mechanical testing. Our analysis confirmed that Ex-4 nanofiber matrices enhanced tendon healing and reduced fibrocartilage formation versus nanofiber matrices alone. These findings implicate Ex-4 as a potentially valuable tool for tendon tissue engineering.

Peer review under responsibility of KeAi Communications Co., Ltd.

* Corresponding author. Department of Orthopedic Surgery Department of Biomedical Engineering Department of Materials Science and Engineering University of Connecticut Health Center N-4052, 263 Farmington Avenue, Farmington, CT, 06030-4037, USA.
E-mail address: Kumbar@uchc.edu (S.G. Kumbar).

https://doi.org/10.1016/j.bioactmat.2023.01.013
Received 11 November 2022; Received in revised form 16 January 2023; Accepted 16 January 2023

1. Introduction

Soft tissues such as tendons and ligaments transmit skeletal force to enable movement and provide stability. These tissues are always exposed to extreme mechanical loads, and their unique fibrillar nature and intricate structural arrangement allow efficient function [1]. These tissues are also at risk of injuries as a result of overuse, pathology, aging, and trauma. The most frequently reported musculoskeletal injury, tendinopathy, results in functional impairment and persistent pain [2]. In the United States, over 300,000 tendon procedures are performed, and this creates an estimated economic burden of $3 billion every year [1,3]. Current treatments fail to restore function due to poor healing and scarring [1,4–6], as regenerated tissue matrix inflexibility leads to high re-tear probability [7–9]. Surgical tendon reconstruction that utilizes both biological and engineered grafts has advantages but continues to suffer from shortcomings such as poor strength and resorption [1,2]. Engineered tendon grafts present superior mechanical and degradation properties over biological grafts, but lack desirable bioactivity to promote tissue healing [1,2].

The ultimate goal of tissue engineering and regenerative medicine is to design bioactive scaffolds that mimic the structure and function of the extracellular matrix (ECM) to improve tissue regeneration and restore function [2,10]. A wide range of natural and synthetic polymers and decellularized tissue have been processed into 3D scaffolds that each have benefits and disadvantages [2]. These scaffolds should ensure mechanical properties to withstand the load at the defect site, promote cell-material interaction, and have biocompatible degradation byproducts to suppress immune responses [2,10,11]. *Polyesters including poly (lactic acid) (PLA), poly(glycolic acid) (PGA), and their copolymers poly (lactic-co-glycolic acid) (PLGA) have been widely explored as a scaffold* and drug delivery material platforms [12,13]. These materials offer excellent initial mechanical strength and short-term biocompatibility, *but are known to compromise tissue healing due to acidic degradation byproducts—this results in premature implant failure as a result of bulk degradation* [2,14,15]. Bioactive natural polymers and proteins are water-soluble, and generating 3D scaffolds from these materials requires cross-linking to stabilize the structure; however, these are often mechanically suboptimal for tendon tissue regeneration [2,14,16]. Efforts to combine the beneficial features of both synthetic and natural polymers can create mechanically stable bioactive scaffolds for tissue regeneration [14].

The physiochemical properties of the polymer dictate the scaffold fabrication process and ultimately scaffold properties [17,18]. Electrospinning has emerged as a simple and scalable technique to produce polymeric fiber matrices for a variety of biomedical and high-technology applications [10,14,16]. These fiber matrices have proven particularly beneficial for regenerating a variety of soft tissues due to their close structural resemblance to native ECM [19]. This process allows the creation of fiber matrices with diameters ranging from 100 nm to 5 μm with high surface area and porosity [10,14,16]. However, certain electrospun nanofiber matrices such as PLGA are known to shrink dimensionally upon exposure to biological fluids and lose intact fiber structure [20]. This structural change compromises mechanical strength, cell-material interactions, and regeneration. The PCL nanofiber matrices do not undergo structural deformation but are hydrophobic, which limits cell-material interaction leading to cell detachment [14,21,22]. In our previous work, we have shown ways to overcome electrospun PLGA fiber matrix shrinkage and PCL matrix hydrophobicity by adding 10–20 wt % cellulose acetate (CA) to the electrospinning solution [14,20]. The PCL-CA blend nanofiber matrices resulted in enhanced hMSC attachment, proliferation, and tenogenic differentiation as compared to control PCL nanofiber matrices [14].

Electrospun polymeric nanofiber matrices have been engineered to deliver bioactive molecules, in the form of growth factors and drugs, to promote and modify tissue healing responses [11,22,23]. The high surface area of these matrix formulations enhances the water solubility of these poorly water-soluble drugs [11]. Delivery of growth factors and other hydrophilic drugs is often very short-lived due to poor encapsulation efficiency, preferential accumulation of factors on the fiber surface, smaller fiber diameter, and high surface area culminating in dose dumping [11,13,24]. The majority of the encapsulated drug is released in the first few hours, which defeats the purpose of controlled release over an extended time to promote regeneration [25,26]. Efforts were also made to chemically tether growth factors and drugs to electrospun nanofibers to sustain their release, but there are remaining challenges in terms of poor factor loading and loss of bioactivity in the process [27]. We previously employed naturally occurring halloysite nanotubes (HNTs) to carry a highly water-soluble drug, 4-aminopyridine, and showed the feasibility of its extended-release from a scaffold over 8 weeks [28,29]. Mixing the drug-loaded HNTs into a polymer solution before electrospinning enables efficient physical drug loading in the nanofiber matrix [30]. Additionally, since the drugs are carried inside the HNTs, the polymer seals tube endings to protect the drug from premature release and degradation, allowing for sustained release [30–32].

Stimulating the tenogenic differentiation of stem cells is important for regenerating tendons, but there is a lack of FDA-approved growth factors or well-defined induction media for promoting stem cell tenogenic differentiation. Studies have used biochemical [16,33], mechanical [34], or structural [35,36] cues and their combination [17,37] to promote the tenogenic differentiation of stem cells. Multiple growth factors (GFs) have been explored to initiate molecular signaling to regulate cell adhesion, proliferation, migration, and differentiation [12,38], but GFs are large and have short half-lives. Small molecule drugs and peptides are stable, and inexpensive, and have been explored as growth factor alternatives to promote stem cell tenogenic differentiation [14,39]. Recently, we have established the benefits of Exendin-4 (Ex-4), a synthetic analog to glucagon-like peptide-1 (GLP-1), in promoting the tenogenic differentiation of hMSCs as compared to other exploratory factors [40]. Ex-4 is a drug to treat type II diabetes but is known to cause hypoglycemia and nausea at improper doses and has a half-life of 3–5 h [41,42]. Repurposing Ex-4 as a tenogenic agent requires an implantable drug delivery system that eliminates the need for repeated systemic administration, maintains release at a safe, functional level, and promotes regeneration [41,42].

In this study, we describe the design, development, and characterization of an Ex-4 encapsulation within halloysite nanotubes (HNTs) PCL-CA blend nanofiber matrix formulation for tendon regeneration. We characterize the nanofiber matrix for its morphology, mechanical strength, and in vitro drug release behavior. We study the effect of Ex-4 present in the nanofiber matrix in regulating hMSC adhesion, proliferation, and tenogenic differentiation in vitro. We further evaluate the efficacy of using the fiber matrix to surgically repair full-thickness rat Achilles tendon defects.

2. Materials and methods

Poly(caprolactone) (PCL; Mw-80kD), cellulose acetate (CA; Mw-50kD), halloysite nanotubes (HNTs), fluorescein isothiocyanate (FITC), papain, other salts, and analytical grade solvents were purchased from Sigma-Aldrich (St. Louis, MO). Human mesenchymal stem cells were purchased from RoosterBio Inc. (Frederick, MD) and Dulbecco's minimum essential medium (DMEM) media from Lonza Bioscience (Morrisville, NC). All cell culture supplies including pen-strep (P/S), fetal bovine serum (FBS), dialysis bags, L-cysteine hydrochloride, 0.25% trypsin EDTA, Quant-iT™ PicoGreen™ dsDNA Assay Kit, and Cell Titer 96® AQueous One Solution Cell Proliferation Assay were purchased from Fisher Scientific (Fair Lawn, NJ). QIAzol Lysis Reagent and RNeasy Plus Mini kit were purchased from QIAGEN Inc. (Germantown, MD) while iScript cDNA Synthesis Kit and iTaq Universal SYBR Green Supermix were purchased from Bio-Rad (Hercules, CA). Exendin-4 (Ex-4) was purchased from AnaSpec Inc. (Fremont, CA), and insulin was

purchased from ProSpec Inc. (East Brunswick, NJ).

2.1. Scaffold preparation and characterization

2.1.1. Halloysite nanotube drug loading

Ex-4 incorporation into the open lumen of HNTs was carried out as per our previous work [29]. In brief, an aqueous 1 mg/mL Ex-4 stock solution and HNTs were (1:1 vol ratio) sonicated for an hour in the bath sonicator. This suspension was further subjected to cyclic vacuum pumping in/out overnight to replace the air in the HNT lumen with Ex-4 solution. Drug-loaded HNTs were collected by centrifugation (6000 rpm) for 20 min and washed with DI water three times. The Ex-4-loaded HNTs were freeze-dried for 24 h and kept desiccated until further use. The drug loading efficiency (DL) was calculated using Equation (1) below. Where $W_{initial}$ and W_{final} are the initial and final weights of the Ex-4 loaded HNTs used for estimations. Extracted Ex-4 concentrations from HNTs were determined using a UV-Spectrophotometer (Genesys 10S, Thermo Fisher Scientific, Waltham, MA, USA) and the absorbance was read at 283 nm.

$$\%DL = \frac{W_{final}}{W_{initial}} \times 100 \qquad \text{Equation-1}$$

2.1.2. Electrospinning

A 12.5% wt./v of PCL and CA at an 80:20 w/w ratio were prepared in 2,2,2-trifluoroethanol and electrospun at ambient conditions. The optimized spinning parameters included a flow rate of 2 mL/h, a working distance of 20 cm, an applied voltage of 16 kV, and a 10 G needle to obtain bead-free nanofibers [14,43]. Random nanofibers were collected on the aluminum rotating target at 20 rpm and kept desiccated until further use. Similarly, Ex-4 loading was performed by mixing a 2.5% wt./wt. (dry polymer weight) of Ex-4 or HNT-Ex-4 to the spinning solution and spun under identical conditions as control nanofiber matrices described above. Drug-loaded nanofiber matrices were stored at −20 °C until further use.

2.1.3. Nanofiber scaffold surface characterization

The morphology of the electrospun nanofiber matrices was imaged using scanning electron microscopy (SEM) (JEOL JSM-6335F, JEOL USA, Inc., MA, USA) at various magnifications. Nanofiber matrices were coated with Au/Pd using a sputter coater (Polaron E5100, Quorum Technologies, East Sussex, UK) before imaging. Images obtained at 1000X were used to measure fiber diameter and pore size. For each formulation, 3 different samples were selected and imaged at 5 different locations. The reported values are an average of 100 different measurements.

2.1.4. Characterization of HNTs within nanofiber matrices

To visualize Ex-4 carrying HNTs within the nanofiber matrix, fluorescent microscopy was employed. A fluorescent dye (FITC) was used in place of Ex-4 and nanofibers were produced as explained above. These nanofibers were collected on the glass cover slide and imaged at 40× magnification using a fluorescence microscope (Nikon Eclipse TS100).

2.1.5. In vitro Ex-4 release

The Ex-4 release patterns for different nanofiber formulations were carried out in PBS pH 7.4 at 37 °C using an orbital shaker. In brief, nanofiber matrices weighing ~20 ± 2 mg were placed in dialysis bags (MWCO 6000–7000) with 1 mL PBS, tied, and incubated in 7 mL of PBS in 15 mL Eppendorf tubes to maintain a sink condition. At different time intervals, 1 mL of the dissolution was collected, replenished with fresh PBS, and quantified using a UV–Vis spectrophotometer at 283 nm.

2.1.6. Tensile property measurement

Tensile properties of nanofiber matrix with and without Ex-4-HNTs were evaluated to identify potential differences. Nanofiber matrices were cut into dog bone shapes (n = 6) maintaining the dimensions 1:2 ratio (diameter: length) and incubated overnight in PBS at 37 °C before testing as specified in ASTM D882-18. Instron 3300 Single Column Universal Testing System (Instron, Norwood, MA, USA) was used for these measurements at a strain rate of 5 mm/min until failure. Using the stress-strain curve, matrix tensile strength, maximum load, and Young's modulus were calculated.

2.2. In vitro bioactivity assessment: cell culture experiments

2.2.1. Human mesenchymal stem cell culture

hMSCs were expanded as per the instructions provided by the vendor. In brief, hMSCs were cultured in DMEM growth media supplemented with 10% FBS and 1% P/S and media in a 150 mm dish, and the medium was changed every three days until cells reached 90% confluency. These cells between passages 3–4 were used for subsequent characterizations.

2.2.2. Culturing of hMSCs on nanofiber matrices

Nanofiber matrices (1 cm^2) were sterilized by immersion in 70% ethanol, washing with PBS, and UV light exposure as per published work [44]. These sterile scaffolds were transferred into non-treated 48-well plates and each scaffold was seeded with 30,000 cells as per the optimized conditions [44].

2.2.3. Cell viability

The initial hMSCs viability and morphology on the nanofiber matrices were assessed by Live/Dead staining and imaging [12,14]. At 1 and 3 days post-seeding, media was aspirated, scaffolds (n = 3/type) were washed with PBS three times and stained according to the manufacture's protocol [12,14]. The green staining represents live cells while the red staining represents dead cells.

2.2.4. The short-term hMSC proliferation: metabolic activity

The metabolic activity of the hMSCs seeded on the nanofiber matrices was evaluated using a Cell Titer 96® AQueous One solution cell proliferation assay [40]. The control groups included hMSC-seeded nanofiber matrices (without Ex-4) cultured in media with or without 20 nM Ex-4. At predetermined time points of 0.25, 3, and 7 days, media was aspirated, matrices (n = 3/type) were washed with PBS, and a fresh, serum-free media was added followed by MTS (tetrazolium) reagent in 10 μL/100 μL ratio for the media and kept incubated for 2 h in the cell incubator. The color intensity of the reaction media was read at 490 nm on a plate reader.

2.2.5. The long-term hMSC proliferation: DNA quantification

The DNA content as a function of time over 21 days was measured using the PicoGreen assay [40]. The control groups included hMSC-seeded nanofiber matrices (without Ex-4) cultured in media with or without 20 nM Ex-4. Cellular constructs at 1, 7, 14, and 21 days were isolated (n = 3/type), washed with PBS, and stored at −80 °C. At the end of the study, cells were enzymatically digested in papain buffer overnight at 65 °C. The cell lysate was used to perform the assay as per the instructions provided with the assay kit [14,40].

2.2.6. Sulfated glycosaminoglycan synthesis: dimethyl methylene blue (DMMB) assay

Sulfated glycosaminoglycan (s-GAG) is a major marker in tendon physiological processes and supports regeneration [15,43]. The cell lysate obtained for the DNA assay was used for the DMMB assay as per the published protocol [14,45]. In brief, 50 μL of cell lysate (n = 3/Type) and 200 μL of DMMB reagent were combined and the absorbance of samples and standards were read at 520 nm [45].

2.2.7. Collagen synthesis: hydroxyproline assay

Collagen synthesis is considered to be an important marker during

tendon regeneration [40,46]. The total collagen synthesized by hMSCs was measured using hydroxyproline assay as per published protocols [46]. In brief, 50 μL of cell lysate (n = 3/type) was hydrolyzed using 100 μL of 6 N hydrochloric acid at 110 °C overnight and dried at 65 °C in the fume hood. The dried samples were dissolved in 200 μL DI water. To a 60 μL sample, 20 μL of assay buffer and 40 μL of chloramine-T reagent were added and allowed to stand for 15 min at room temperature. To this mixture, 80 μL of DMBA reagent was added and samples were incubated in a water bath at 60 °C for 20 min before reading the optical density at 570 nm [40,46].

2.2.8. Tenogenic markers: gene expression

Tenogenic gene expression by hMSCs under different treatment conditions as a function of time over 21 days was measured using quantitative polymerase chain reaction (qPCR). To collect a higher quantity of RNA, each matrix and control were seeded with 100,000 cells (n = 4/treatment). RNeasy Plus Mini Kit and QIAzol/chloroform extraction methods were employed to extract RNA [14,40]. At 7, 14, and 21 days post cell seeding, each scaffold was aseptically transferred from the media into sterile tubes, QIAzol was added, and samples were stored at −80 °C. Once all the samples were collected, chloroform was added to each tube at a ratio of 210 μL of chloroform to 900 μL of QIAzol followed by centrifugation at 10,000 rpm for 20 min at 4 °C. The collected RNA layer was dissolved in an equal volume of absolute ethanol and transferred to an RNeasy spin column to further process according to kit instructions. The quality and the quantity of RNA were determined using a NanoDrop spectrophotometer. 500 ng of RNA was reverse transcribed using an iScript cDNA synthesis kit, and iTaq SYBR green kit was used for PCR using a BioRad CFX96 machine. The primer sequences are listed in Table S1 [40]. The tenogenic genes such as tenomodulin (Tnmd), scleraxis (Scx), and mohawk (Mkx), as well as ECM-related genes collagen type-I (Col-I), collagen type-III (Col-III), and decorin (Dcn), were quantified and normalized to the glyceraldehyde 3-phosphate dehydrogenase (GAPDH) housekeeping gene.

2.3. In vivo assessment

2.3.1. Isolation of MSCs from rat long bones

Female, 10-week-old Sprague-Dawley (SD) rats were euthanized to harvest MSCs (rMSCs) from long bones following a previously published protocol for cell therapy [47]. In brief, long clean bones without surrounding soft tissues were washed with 70% ethanol and moved to a tissue culture hood in sterile PBS. These bones were cut on the edges and marrow was flushed out with DMEM using an 18-gauge needle. The contents were filtered through a 20 μm filter and centrifuged to separate red blood cells from stromal mesenchymal stem cells. The rMSCs fractions were cultured in 10 mm tissue culture plates, expanded, and passage 2 cells for use as donor cells in transplantation.

2.3.2. Labeling MSCs for tracking

Tracking donor rMSCs following transplantation was enabled by fluorescent membrane labeling using ViaFluor® SE Cell Proliferation Kit as per instructions. Two different dye concentrations namely 1 μM and 2.5 μM were used and cultured in 10 mm plates and fluorescent images were taken over 12 weeks. Long-term detectable dye concentration was used to label the donor cells 24 h before surgery.

2.3.3. Scaffolds seeded with donor cells for transplantation

Nanofiber matrices (PCL-CA with HNT-Ex-4) with the dimensions of 5 × 10 mm were sterilized and seeded with labeled donor rMSCs at a density of 1,000,000 cells/scaffold and used for transplantation after 24 h.

2.3.4. Animal study design

One hundred fifty (150) female 12-week-old Sprague Dawley rats (Charles River Laboratories, Wilmington, MA) were randomly divided into six groups: sham, no repair, suture, scaffold, scaffold with Ex-4, and scaffold with Ex-4 seeded with rMSCs. All animals were housed in groups of four before the surgical procedure, where food and drink were provided at a controlled room temperature with a 12-h light-dark cycle. All animals were allowed to acclimate to the housing environment for up to one week before surgery. The animal care protocol was approved *(protocol number 101531-1219)* by the Institutional Animal Care and Use Committee (IACUC) at the University of Connecticut, and the National Institutes of Health regulations and standards for animal usage were followed.

2.3.5. Surgical procedure

Rats were anesthetized via inhaling isoflurane and oxygen. Body temperature was maintained at 37 °C using a surgical warm pad placed underneath the rat. All surgeries were conducted in the surgical suite using sterile surgical tools. The left hind leg was shaved and cleaned with betadine and isopropanol alternatively three times. A 15 mm incision was made over the Achilles tendon (Fig. S1). As the Achilles tendon was identified, it was dissected carefully, and surrounding tissues were cleared. The Achilles tendon was damaged via full-thickness transection and the calcaneus tendon was removed. These defects were treated as explained in the study design. For the sham group, the tendon was exposed without damaging it. In the no-repair group, the damaged tendon was not repaired. For the suture group, the Achilles tendon was sutured with 6–0 Proline suture (Ethicon Inc., Somerville, NJ). A 5 × 10 mm^2 scaffold was wrapped tightly around the tendon and secured via a 6-0 Proline suture in scaffold-treated groups. The skin incision was closed using 5-0 Vicryl® suture (Ethicon Inc., Somerville, NJ), cleaned with alcohol wipes, and glue was applied. After the surgery, animals were housed individually, pain was managed via buprenorphine injection every 12–18 h for two days.

2.3.6. Blood serum collection for analysis

Blood serum samples will be collected at 3, 7, and 14 days post-surgery to analyze immune markers and Ex-4 content. A sample size of n = 3 was used for Ex-4 implantation and rMSCs-seeded scaffold groups. The drug content was analyzed using the Exendin-4 ELISA kit (Phoenix Pharmaceuticals, Inc. Burlingame, CA) and IL-6 and IL-10 using ELISA kits (R&D system, Inc. Minneapolis, MN).

2.3.7. DigiGait walking analysis

The functional recovery analysis was assessed following Achilles tendon transection and repair using the DigiGait imaging and analysis system (Mouse Specifics, Inc., Framingham, MA) [28]. The DigiGait system uses unique software that converts video imaging into a computerized paw print. The animals have to walk individually on a speed-controlled treadmill in a closed chamber with an optimum speed (20 cm/s) (Fig. S2). Each rat has to walk continuously for at least 5 s. Every rat was made to walk on the system several times to acclimate to the environment before recording. Each treatment group has n = 8 and a baseline measurement was collected before the surgery. Animals were walked every week for the first 4 weeks post-surgery. The acquired dynamic signals were corrected to optimize the signal-to-noise ratio and digitized to analyze different parameters such as Achilles functional index (AFI), paw area, stance, and stride.

2.3.8. Tissue harvesting and gross morphology

Two weeks and twelve weeks post-surgery, animals were euthanized by carbon dioxide asphyxiation. The repaired Achilles tendons were carefully dissected and washed with PBS. The length and thickness of the tendon (n = 6) were carefully measured using a digital caliper and compared to the native tendon.

2.3.9. Histological evaluation

After euthanasia, the left Achilles tendon was harvested, washed with PBS, and fixed with 10% neutral buffered formalin at 4 °C for two

days. Samples (n = 3) were washed with PBS three times and transferred to 70% ethanol before embedding. Samples were paraffin-embedded, and serial longitudinal sections approximately 5 μm thick at three different depths (100 μm in between) were prepared for histological evaluation (Fig. S3). Hematoxylin and eosin (H&E), Trichrome, and Safranin O staining were performed following their standard protocols. Similarly, immunohistochemistry (IHC) was performed to detect Col-I and Col-III. The slides were imaged using Aperio CS2 high-resolution digital scanner (Leica Biosystems Inc., Buffalo Grove, IL). The H&E evaluation was conducted using a scoring system [48] to evaluate the general morphology according to the six parameters (fiber structure and arrangement, rounding of the nuclei, inflammation, increase vascularity, cell density, and cartilage formation). The assessment was conducted for 24 images in each group per timepoint by three colleagues who were blinded. The final results were confirmed by an expert pathologist. The native tendon would have a 0 total score, while abnormal tissue would have a maximum score of 18. All other quantifications were performed using ImageJ software using at least 6 images per group for IHC, while the other staining analyses had at least 18 images per group. In addition, frozen sections were used to check the donor cells after harvesting. For that, tendons (n = 3) were fixed in 10% neutral buffered formalin at 4 °C for two days, washed with PBS and incubated in 30% sucrose overnight at 4 °C. The tendon then was embedded in cytomatrix and stored at −80 °C overnight. Samples were cryosectioned (5 μm) using a cryostat tape transfer system (Section-lab, Hiroshima, Japan) [49]. The acquired sections were imaged using a confocal microscope.

2.3.10. Gene expression PCR

Harvested tendons for PCR were placed in Rino 1.5 ml screwcap tubes with beads and 500 μl QIAzol was added. The samples were vigorously crushed using bullet blender homogenizers (Next Advance, Inc. Troy, NY) at the highest speed (12) for 5 min. The samples were then stored at −80 °C until the end of the study. The RNA extraction was conducted following a previous protocol [50]. A 1 μg sample of RNA was reverse transcribed using an iScript cDNA synthesis kit and iTaq SYBR green kit was used for PCR using a BioRad CFX96 machine. Gene expression of tendon-related markers, cartilage-related markers, bone-related markers, as well as immune markers was quantified and normalized to the glyceraldehyde 3-phopsphate dehydrogenase (GAPDH) housekeeping gene. The primer sequences are listed in Table S2 [51–53].

2.3.11. Mechanical testing

At the harvesting timepoint, samples of the repaired tendon as well as the contralateral were collected and stored at −80 °C. The rat's foot was first tightly wrapped with a 0.9 mm diameter steel wire to act as a rebar then fixed in a block of orthodontic resin. Tendon dimensional measurements were taken using a digital caliper. Then muscles were carefully scraped using a scalpel and secured in a custom sinusoidal clamp. The tendon and sinusoidal clamp were freeze-dried using dry ice to prevent sample slippage during load to failure. Mechanical testing was conducted using a servohydraulic materials testing system (MTS 858 Bionix II; MTS Systems Corp) with a 100 N axial load cell to measure tendon failure force. The uniaxial tensile tests were performed at a rate of 5 mm/min with a 1 N preload. Load-to-failure data was recorded, and stiffness was calculated from the liner region of the curve. The stress-strain curve was constructed. The tensile stress and young modulus were calculated.

2.3.12. Statistical analysis

For all experiments, an adequate sample size was used based on the power analysis. All quantification assays and image analyses used a sample size of n = 3/timepoint and gene analysis used n = 4/timepoint. Results are expressed as means ± standard deviation (SD). Statistical analysis was carried out using one-way ANOVA followed by Tukey's post hoc analysis for multiple comparisons to determine significance using GraphPad Prism software (GraphPad Software, Inc. La Jolla, CA). A value of $p < 0.05$ was considered significant.

3. Results

3.1. Halloysite nanotube drug loading and scaffold characterization

Naturally occurring halloysite nanotubes measure ~50 nm outer diameter, 600–900 nm in length, and 15 nm inner diameter (lumen), and eliminate from the body in their native form [28,31,32]. The outer surface of the HNT is made of SiO_2 and is negatively charged, while the lumen is made of $Al(OH)_3$ and is positively charged [31,32]. Because of this variable stoichiometry, surface charge, and functional groups, HNTs present advantages for physical or chemical drug incorporation [29,54]. At physiological pH, negatively charged Ex-4 is more likely to be held in the HNT lumen by electrostatic forces of attraction [41,42]. The Ex-4 encapsulation efficiency was found to be 8.7 ± 0.3%, which is consistent with our previously reported chitosan scaffold system [31,32].

At the optimized electrospinning parameters, polymer and HNT doping concentrations produced bead-free micron- and nano-sized randomly oriented fibers. Fig. S4 illustrates general fiber morphology and the micro-nano fiber random orientation. Fiber diameters in the matrix showed a typical Gaussian distribution with an average of 1.0 ± 0.2 μm and 1.3 ± 0.3 μm for neat polymeric and with HNT-Ex4, respectively. Similarly, these matrices had average pore sizes of 3.1 ± 0.7 μm and 2.5 ± 0.5 μm, respectively. Observed differences in fiber diameter and pore sizes in control and drug-loaded fiber matrices are due to the addition of HNT-Ex-4 to the polymeric solution of identical concentration. In our previous studies, we showed the advantages of these matrix parameters and their applicability in controlling cell-material interactions [30,54,55].

Fluorescent microscopy was used to visualize the presence of drug-carrying HNTs within individual fibers of the fiber matrix. Fig. S5 shows the physical blending of FITC fluorescent dye and HNT-FITC distribution within fibers. A noticeable change in the dye distribution intensity and pattern identifies the presence of drug-carrying HNTs. In the case of HNTs carrying the dye, the discontinuous appearance of fluorescence in small segments confirms HNT encapsulation within the polymeric fibers. Hollow fibers with the continuous presence of FITC on the fiber surface were seen for freely doped FITC within the scaffold.

3.2. Drug release

For the fiber matrices carrying free-form Ex-4 encapsulation efficiency (EE) was 34.4%. It means only 34.4% of the free drug was retained within nanofibers and the rest was lost during the electrospinning process. However, a higher EE of 86.58% for HNT-Ex-4 fiber matrices was due to drug protection within HNT, and tube endings were closed with the polymer solution during electrospinning. Fig. S6 illustrates the in vitro drug release pattern from both formulations where HNT-Ex-4 reduced burst release from ~75% to ~40%. This is a significant improvement in overcoming the dose-dumping issues of nanofiber matrices to provide sustained release. As such, HNTs as drug carriers release the majority of the drug within 4–12 h [31,32], but sealed tube endings by the polymer in fiber matrices sustain the release over an extended period [29].

3.3. Release kinetics modeling

Ex-4 release from both fiber matrices was fit to Zero Order, First Order, Hixson-Crowell, Higuchi, and Korsmeyer-Peppas (K–P) release kinetics models [56]. The different parameters from these models are presented in Table S3. The correlation coefficient (R^2) for Higuchi and K–P models appears to fit very well for the release pattern. The release exponent (n) value in K–P $n < 0.5$ for both formulations indicate quasi-Fickian diffusion suggesting partial Ex-4 diffusion [25,29].

3.4. Tensile testing

Fig. S7 summarizes wet fiber matrix tensile properties, namely elastic modulus, tensile strength, and maximum load at failure. Fiber matrices with Ex-4 and HNT-Ex-4 presented average elastic moduli of 31.0 ± 5.2 and 27.6 ± 8.5 MPa; tensile strengths of 23.3 ± 3.8 and 18.6 ± 4.1 MPa; and maximum loads of 3.1 ± 0.5 and 2.5 ± 0.5 N, respectively. HNT doping did not significantly affect the tensile properties of drug-loaded fiber matrices.

3.5. Cellular attachment, viability, and proliferation

The ability of our bioactive fiber matrices to support hMSC attachment and proliferation over a short period is an early indication of its cytocompatibility. Fig. 1A summarizes cell proliferation over 7 days as determined by MTS assay. The hMSCs seeded on fiber matrices with HNT-Ex4 were compared to cells seeded on PCL-CA matrices receiving either continuous treatment with 20 nM Ex-4 (positive control) or vehicle media (negative control). Our results illustrate comparable cellular viability to continuous treatment at early time points (0.25 and 3 days) followed by a significantly higher proliferation rate at day 7 for cells seeded on fiber matrices with HNT-Ex4 compared to both controls. The fiber matrices supported the attachment and proliferation irrespective of the presence of Ex-4 in the matrix or the media. The live/dead assay presented in Fig. 1B further confirms the cell viability and their fibroblastic morphology confirming matrix cytocompatibility. The long-term cell proliferation trend under identical test conditions was evaluated by DNA assay and findings are summarized in Fig. 1C. All the matrices supported cell growth as a function of time with significantly higher cell numbers on day 14 on the HNT-Ex-4 matrices as compared to both controls. These results confirm the safe dose and release kinetics of Ex-4 that did not affect cell attachment, viability, and proliferation.

3.6. Sulfated-glycosaminoglycan (s-GAG) and collagen content

The bioactivity of the fiber matrix with HNT-Ex-4 is confirmed by its ability to induce cultured hMSCs into the tenogenic lineage, which was evaluated by quantifying two major ECM components of tendons, namely s-GAG and collagen. Fig. 1D summarizes s-GAG synthesized by cells cultured on fiber matrices under different test conditions. The fiber matrix with HNT-Ex-4 resulted in a significantly higher amount of s-GAG as compared to positive and negative control groups. Similarly, Fig. 1E summarizes cell-produced collagen on fiber matrices under different test conditions. The fiber matrix with HNT-Ex-4 and Ex-4-treated (positive control) resulted in higher collagen content than basal media (negative control) at both time points. This further confirms the bioactivity of fiber-matrix-eluted Ex-4 promoting hMSCs tenogenic differentiation comparable to the positive control. A significantly higher

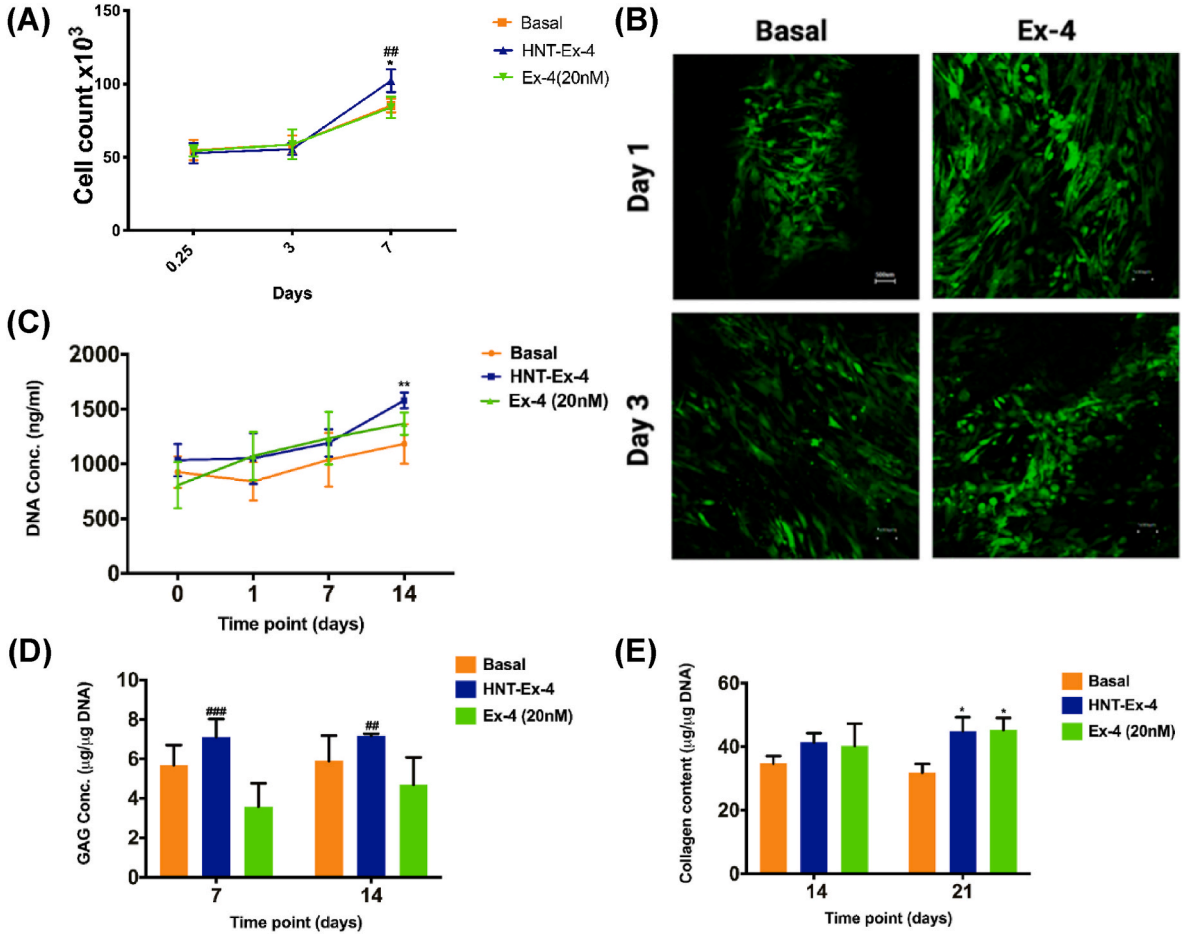

Fig. 1. Nanofiber matrices with HNT-Ex-4 supported high hMSC proliferation and viability, and high collagen and GAG production. (A) hMSCs proliferation as determined by MTS assay **with and without Ex-4.** Control PCL-CA matrices treated with media containing 20 nM Ex-4 (positive) and without Ex-4 (negative; Basal). *p < 0.05 vs negative control; ##p < 0.01 vs Ex-4(20 nM). Live/Dead assay confocal images (10X). **(B)** hMSCs viability over 3 days on the neat PCL-CA scaffold and with HNT-Ex-4. The scale bar is 500 µm. **(C)** On day 14, fiber matrices with HNT-Ex-4 had a higher hMSC proliferation rate than both controls (20 nM Ex-4 and no Ex-4 [Basal]). **p < 0.01 vs negative control. **(D)** S-GAG assay: At days 7 and 14, fiber matrices with HNT-Ex-4 had higher hMSC proliferation rates than both controls (20 nM Ex-4 and no Ex-4 [Basal]). ##p < 0.01 vs Ex-4 (20 nM). **(E)** The amount of total collagen on fiber matrices with HNT-Ex-4 was higher than media without Ex-4 (negative control; Basal) and comparable to 20 nM Ex-4 (positive control). *p < 0.05 vs negative control.

level of collagen synthesis by Ex-4-treated cells as compared to basal media (negative control) at day 21 further confirms its optimal dose to promote tenogenic differentiation.

3.7. Tenogenic gene expression

The HNT-Ex-4 fiber matrix induced cultured hMSCs into the tenogenic lineage as indicated by the expression of tendon-related genes, including mohawk (Mkx), scleraxis (Scx), and tenomodulin (Tnmd), as well as ECM proteins decorin (Dcn), Col I, and Col III. Fig. 2 summarizes the relative expression of these genes compared with basal media (negative control) over time. All these genes were expressed for the test group and positive control but their expression trend varied with time. Fiber matrices with HNT-Ex-4 and Ex-4 treatment (positive control) exhibited significantly higher levels of Col-I at day 7 as compared to basal media (negative control). On day 14, fiber matrices with HNT-Ex-4 expressed significantly higher levels of Col-I as compared to controls. Similarly, Col-III expression on fiber matrices with HNT-Ex-4 was significantly higher on days 7 and 21 as compared to basal media. The Ex-4 treatment (positive control) significantly enhanced Col-III expression on days 14 and 21 as compared to basal media. The relative ratio of Col-I to Col-III expression was 1.279 ± 0.174 for HNT-Ex-4 on day 7 and significantly elevated to 3.024 ± 0.938 on day 14. Expression of Mkx, Scx, and Tnmd was significantly higher for all groups as compared to basal media (negative control). HNT-Ex-4 and Ex-4-treated fiber matrices demonstrated significant upregulation of Mkx at day 7, while HNT-Ex-4 matrices also had significant upregulation at day 21. Similarly, Scx expression was significantly increased compared to negative controls on days 7 and 14 on fiber matrices with HNT-Ex-4, while matrices treated with Ex-4 had significantly increased expression on days 14 and 21. However, expression of Tnmd was significantly upregulated at days 14 and 21 for cells cultured on fiber matrices with HNT-Ex-4 as compared to both controls. Significantly higher levels of Dcn were seen for fiber matrices with HNT-Ex-4 and Ex-4 treatment at day 7 as compared to basal media (negative control). Expression of Dcn peaked on fiber matrices with HNT-Ex-4 at day 21 as compared to both controls.

3.8. Donor cells harvesting and membrane labeling

Rat mesenchymal stem cells (rMSCs) were successfully harvested, isolated, and expanded for cell therapy. It is important to track the fate of donor cells and investigate their impact on tendon healing. Therefore, the cell membrane was labeled using a well-known proliferation dye kit (ViaFluor SE proliferation kit) that interacts with the cell membrane's protein to activate the fluorescence. As the cells divide, the intensity of the dye will be reduced over time. We investigated two concentrations of the fluorescent dye and tracked the cells for 12 weeks in vitro (Fig. S8). We successfully traced rMSCs for 12 weeks using 2.5 μM concentration.

3.9. Rat achilles tendon defect procedure

The study included 12 animals in each group per timepoint. The surgical procedure is provided as a supplemental figure (Fig. S1). All rats remained healthy the whole study without any complications.

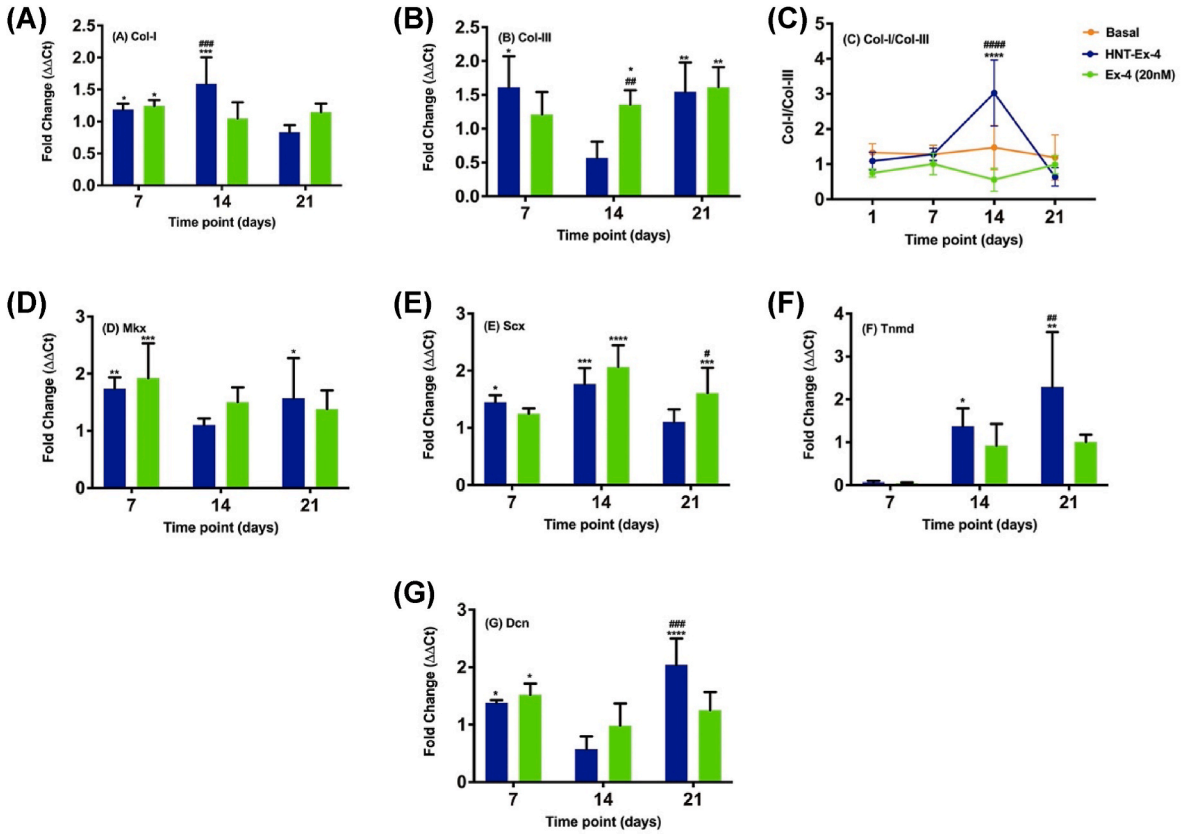

Fig. 2. Fiber matrices with HNT-Ex-4-induced hMSC expression of tendon-related genes. Expression of mRNA by hMSCs seeded on PCL-CA scaffold with HNT-Ex-4 (blue) or groups treated with 20 nM Ex-4 (positive control, green) compared to hMSCs seeded on neat scaffolds in media without Ex-4 (negative control; Basal) (n = 3). Time course pattern for genes: (A) Collagen-I (Col-I), (B) collagen-III (Col-III), (C) ratio of Col-I and Col-III, (D) mohawk (Mkx), (E) scleraxis (Scx), (F) tenomodulin (Tnmd), and (G) decorin (Dcn). Data are presented as mean ± SD. *p < 0.05, **p < 0.01, ***p < 0.001, and ****p < 0.0001 vs negative control. #p < 0.05, ##p < 0.01, ###p < 0.001, and ####p < 0.0001 vs continuous treatment of Ex-4 20 nM.

3.10. Systemic detection of immune response and Ex-4 release

To investigate the implication of implanted scaffold as well as the donor cells, blood samples were drawn before the surgery and 1-, 3-, 7-, and 14 days post-surgery. Serum was collected from the following groups: scaffold with Ex-4 and scaffold with Ex-4 and rMSCs and compared to normal rats as control. Exendin-4 release and immune markers – such as proinflammatory marker interleukin-6 (IL-6) and anti-inflammatory marker interleukin-10 (IL-10) that represent macrophage type-1 (M1) and macrophage type-2 M2, respectively – were evaluated in vivo. M1 macrophages are known to mediate inflammation, while M2 macrophages are responsible for repair processes. The results demonstrated a significant reduction in IL-6 level at day 3 for the scaffold + Ex-4+rMSCs group, and at day 7 for the scaffold + Ex-4 group compared to normal rats. At day 14, both groups showed significant elevation in IL-10 level compared to normal rats (Fig. 3).

To monitor the Ex-4 release during the study, we tracked the Ex-4 serum level using an ELISA. The scaffold + Ex-4+rMSCs group showed a significantly higher level of Ex-4 release at all selected time points compared to the control, while the scaffold + Ex-4 group demonstrated significant elevation of Ex-4 level at days 3 and 7 compared to the control (Fig. 4).

3.11. Gross morphology

Tendon morphology was evaluated at weeks 2 and 12. The scaffolds for all groups treated with scaffolds remained in their surgical location (Fig. 5A). At week 2, all groups, excluding the sham group, showed a significant increase in tendon length and cross-section area compared to the native tendon. Twelve weeks post-surgery, the suture and scaffold + Ex-4 groups exhibited a similar range of native tendons in the cross-section area. The average tendon length of the scaffold + Ex-4 group was within the range of the native, while the rest showed a significant increase in length compared to the native (Fig. 5B&C).

3.12. Histological evaluation

To thoroughly assess tendon histology, Hematoxylin & Eosin (H&E) staining (Fig. 6A) was used to evaluate the general morphology using a scoring system. The total score of all groups was significantly higher at weeks 2 and 12 post-surgery compared to the sham group (Fig. S9). At week 12, all scaffold treatment groups exhibited significantly higher total scores compared to the suture group. Cellularity of all groups was significantly elevated at weeks 2 and 12 post-surgery compared to the sham group. It also was observed that all scaffold treatment groups posed significantly higher cellularity compared to no repair and suture groups. The assessment of the fiber structure (collagen grade) and rounding nuclei revealed significant elevation for all groups at week 12 compared to the sham group. Cartilage formation was remarkably evident in the no-repair group at week 12, while all other groups demonstrated significantly lower cartilage formation. The accumulation of inflammatory cells was pronounced in all scaffold treatment groups and the suture group compared to the no repair and sham groups. The neovasculature revealed significant elevation at week 2 for suture, scaffold, and scaffold + Ex-4 groups compared to sham; whereas it demonstrated elevation at week 12 for no repair, scaffold, and scaffold + Ex-4.

Collagen deposition and collagen fibril morphology assessments were performed via Masson trichrome staining (Fig. 6B). Two weeks after implantation, collagen fibers were massively disrupted, and neo-collagen fibrils were formed, as represented by the blue color. All groups except scaffold + Ex-4+rMSCs exhibited a significant increase in the blue staining area compared to the sham group. After 12 weeks, scaffold + Ex-4 and scaffold + Ex-4+rMSCs demonstrated significantly lower aniline staining compared to the no-repair group (negative control) and comparable to the suture group. Red staining, which represents collagen maturation, is remarkably pronounced in the scaffold area at week 12. Semi-quantification of the red staining of suture and scaffold + Ex-4 groups was comparable to the sham group at both timepoints.

The chondrification areas within the defect region were evaluated using safranin O with fast green counter staining (Fig. 6C). At week 12, the histomorphometric quantification of safranin O, represented by the red color, was significantly evident in no repair and scaffold groups; while it was less prominent in suture and scaffold with Ex-4 and donor cell groups. The chondrification area was significantly diminished at week 12 in scaffolds with Ex-4.

3.13. Immunohistochemistry

We further evaluated tendon healing by collagen deposition using the IHC of Col-I and Col-III. At week 2 post-implantation, all scaffold treatment groups demonstrated transient significant increases in Col-III deposition (Fig. 7B) compared to the sham group followed by decreases of Col-III at week 12 for groups treated with scaffold and scaffold + Ex-4. The protein expression of Col-I of all groups was elevated (Fig. 7A). At 12 weeks post-surgery, rats treated with scaffold + Ex-4 demonstrated comparable expression levels of Col-I compared to the sham group. Overall, collagen protein expression suggested a tissue healing path rather than scar formation.

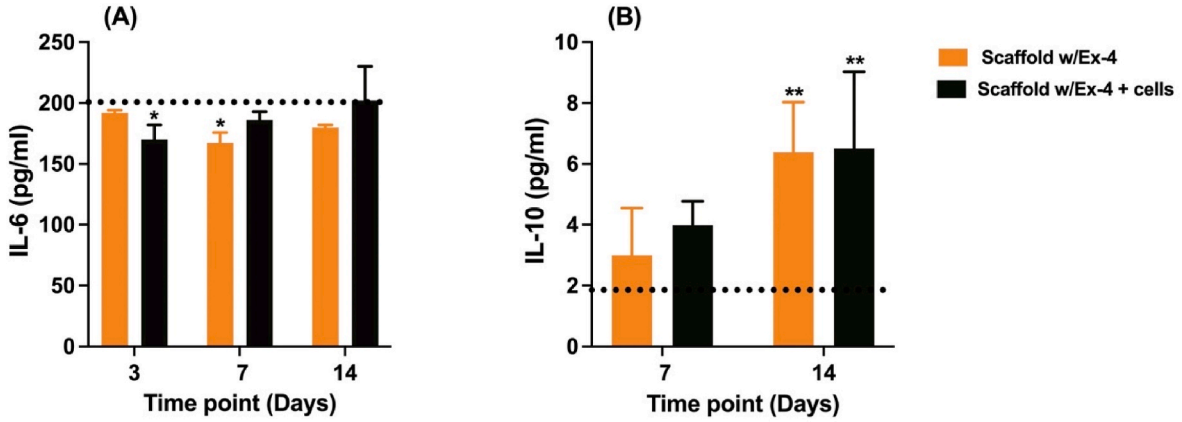

Fig. 3. Rats with Ex-4 scaffold implantation exhibited significantly low IL-6 and high IL-10 levels compared to normal rats. (A) Interlukin-6 ELISA assay (n = 3). (B) Interlukin-10 ELISA assay (n = 3). The dotted black line is normal levels of IL-6 and IL-10 (without treatment). * is $p < 0.05$, and ** is $p < 0.01$ compared to normal rats.

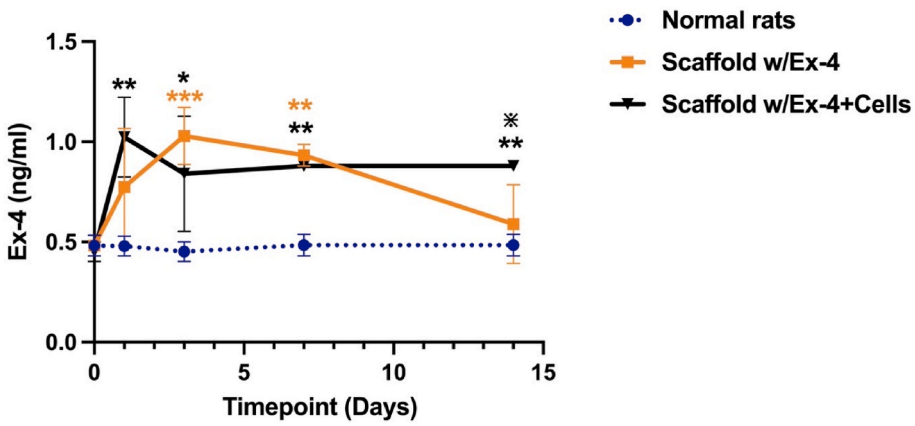

Fig. 4. Rats treated with scaffold w/Ex-4 demonstrated local Ex-4 release one-week post-surgery. Ex-4 concentration detection from serum samples using EIA assay (n = 4). * is $p < 0.05$, ** is $p < 0.01$, *** is $p < 0.001$ compared to normal rats (control). ※ is $p < 0.05$ within tested groups.

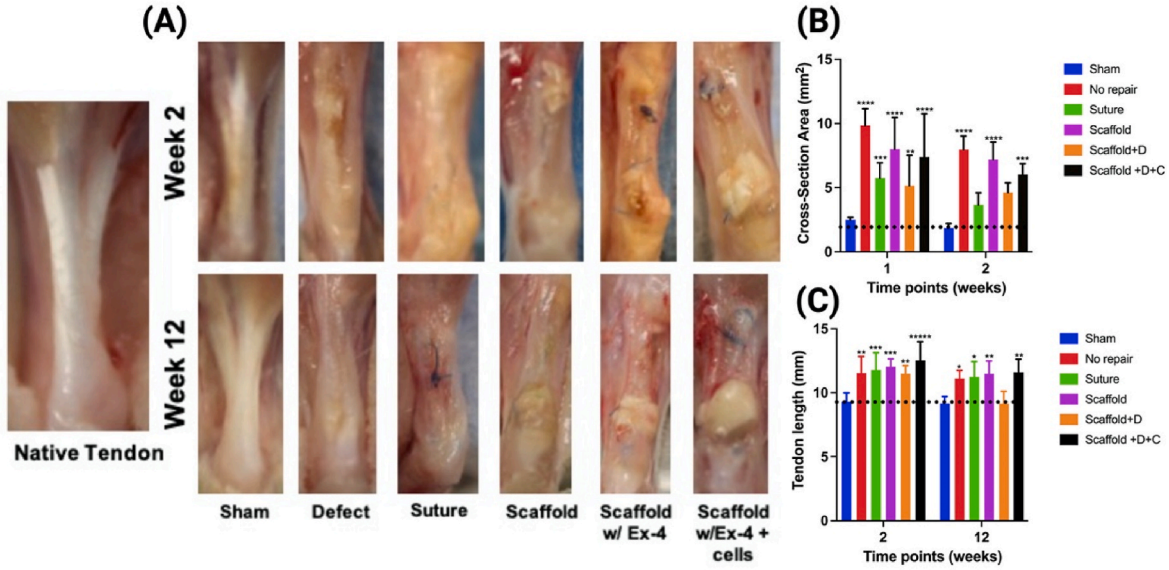

Fig. 5. The implanted scaffold remains in the surgical location. Tendons harvested from rats treated with scaffold loaded with HNT-Ex-4 exhibited cross-section area and tendon length similar to the native tendon. (A)Gross morphology of the harvested rat's Achilles tendon at week 2(top), and week 12 (bottom). (B) Cross-section area of the harvested tendon (n = 4) samples per group in each time point, and compared to the native tendon. (C) Tendon length of the harvested tendon (n = 4) samples per group in each time point, and compared to the native tendon. * is $p < 0.05$, ** is $p < 0.01$, *** is $p < 0.001$, and **** is $p < 0.0001$ compared to the native tissue.

3.14. Donor cell tracking after harvesting

The scaffolds seeded with rMSCs were tracked by looking at fluorescent dye intensity. However, the fluorescent intensity reduced over time due to cell division. Fig. S10 shows a reduced fluorescence intensity at week 12 as compared to week 2**.** Most of the donor cells were confined to the area of injury.

3.15. Gene expression

To understand the tendon regeneration and recovery path post-implantation, we quantified gene expression of a tendon (Fig. 8), bone (Fig. S11), and cartilage (Fig. 9) markers along with immune-related markers (Figs. 10 and 11). Gene expression of tendon-related markers tenomodulin (Tnmd) and scleraxis (Scx) exhibited significant upregulation at weeks 2 and 12 for suture and scaffold + Ex-4 groups compared to sham. Collagen type-I (Col-I) gene expression increased significantly at week 2 for suture, scaffold + Ex-4, and scaffold + Ex-4+MSCs compared to sham, while at week 12 it was significantly elevated for the scaffold + Ex-4 group compared to all groups. The relative expression of Col-III at week 2 was high for the suture group compared to sham, while scaffold + Ex-4 exhibited high expression at week 12 compared to all groups. The gene expression of the ECM-related marker Dcn demonstrated significant upregulation at weeks 2 and 12 for both suture and scaffold + Ex-4 groups compered to sham; whereas ECM-marker tenascin-c (Tnc) was significantly upregulated at week 2 only. The relative expression of tenascin-xb (Tnxb) and fibromodulin (Fmod) showed high expression at week 12 for all scaffold treatment and suture groups compared to sham.

The upregulation of bone-specific markers was evident at weeks 2 and 12 for the repaired group (Fig. S11). At week 2, the suture group demonstrated significant upregulation of alkaline phosphatase (Alp), Smad-1, and Smad-5 genes compared to sham and no repair groups; whereas scaffold + Ex-4 exhibited significant upregulation for Smad-1. At week 12, the scaffold with Ex-4 and MSCs demonstrated significant elevation for bone sialoprotein (Ibsp), Alp, and Smad-1 gene expression. Runt-related transcription factor-2 (Runx2) gene expression was significantly upregulated at week 12 for scaffold and scaffold + Ex-4

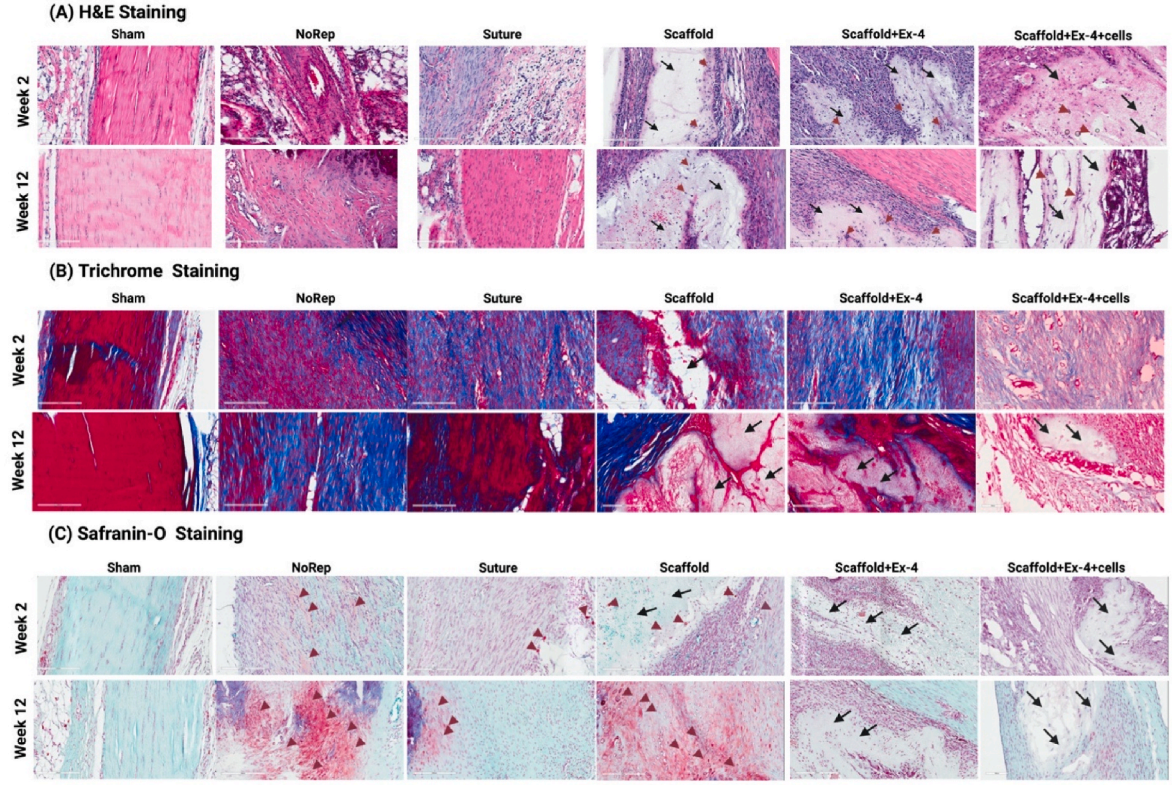

Fig. 6. Representative images of the tendon at the site of injury at 2- and 12 weeks post-surgery. (A) H&E staining. Black arrows label scaffolds while red arrows represent cellular infiltration within the scaffold area. (B) Masson's Trichrome staining. Black arrows label scaffolds. (C) Safranin O staining. The black arrows indicate the scaffold while the red arrows indicate the staining deposition. The scale bar is 200 μm.

groups.

The expression of chondrogenesis-related genes was also altered based on the repair group (Fig. 9). *Aggrecan* (Agn) was upregulated at week 2 for no repair, suture, and scaffold with Ex-4 which was restored 12 weeks post-surgery. The gene expression of collagen type-II (Col-II) was significantly elevated 12 weeks post-implantation for no repair and scaffold groups. Comp gene expression was significantly upregulated for no repair and suture at week 12. Sox-9 demonstrated significant upregulation for no repair, suture, scaffold + Ex-4, and scaffold + Ex-4+rMSCs at week 2 after surgery; however, the normal level of expression was restored 12 weeks post-surgery for all groups except the no repair group.

The mRNA levels of pro-inflammatory cytokines (LY6C, CCL-2, TNF-α, IL-1β, IL-6, CD68) (Fig. 10) were significantly upregulated for suture, scaffold + Ex-4, and scaffold + Ex-4+rMSCs at 2 weeks post-surgery compared to sham. Gene expression levels were attenuated for the suture group at week 12; whereas the gene expression of IL-6, CD68, and TNF-α remained elevated for all scaffold test groups. On the other hand, the gene expression of anti-inflammatory cytokines demonstrated high expression at week 12 post-surgery (Fig. 11). IL-4 gene expression was significantly elevated for suture and scaffold + Ex-4+rMSCs; whereas IL-10 gene expression was significantly upregulated for scaffold + Ex-4, and scaffold + Ex-4+rMSCs compared to the sham group. IL-13 gene expression was significantly increased for scaffold with Ex-4 at both timepoints, while suture and scaffold + Ex-4 groups demonstrated significant upregulation of CD168 at week 2 compared to the sham group.

3.16. Functional recovery analysis

DigiGait treadmill setup used to perform walking gait analysis to evaluate the severity of the injury (Fig. S2). Rats were made to walk on the treadmill before and after the surgery to establish the baseline and recovery via pawprint analysis. DigiGait walking track analysis was used to assess the functional recovery of the injured hindlimb. Different parameters were evaluated including AFI, paw area, stance time, and swing time (Fig. 12). Results were normalized to the contralateral hindlimb. AFI usually ranges from 0 to −120 which indicates normal function to completely impaired function, respectively. One week before surgery, the mean (±SD) AFI was -4.114 ± 6.020. One-week post-surgery, all groups showed significant decreases in AFI ($p < 0.0001$) compared to the sham. All groups demonstrated continuous improvement in the second week. Two weeks post-surgery, rats treated with scaffold + Ex-4 and scaffold + Ex-4+rMSCs demonstrated AFI scores comparable to sham groups.

A paw area of 100% indicates normal paw area while a lower percentage indicates impaired paw area, and all animals scored ~100% before surgery. One-week post-operation, all groups had low paw areas compared to the sham group. Two weeks post-surgery all groups except no repair demonstrated comparable paw area to the sham group. Interestingly, rats treated with scaffold + Ex-4 and scaffold + Ex-4+rMSCs demonstrated significant elevation of paw area compared to no repair.

Swing time and stance time were quantified as part of the functional recovery assessment. Swing time and stance time are inversely related. The swing time increases as dysfunction increases, whereas stance time decreases as dysfunction increases. One-week post-operation, all groups exhibited significant decreases in stance time compared to the sham group. Interestingly, rats treated with scaffold + Ex-4 demonstrated swing time comparable to the sham group after one week. Overall, rats treated with scaffold + Ex-4 or scaffold + Ex-4+rMSCs revealed better functional recovery.

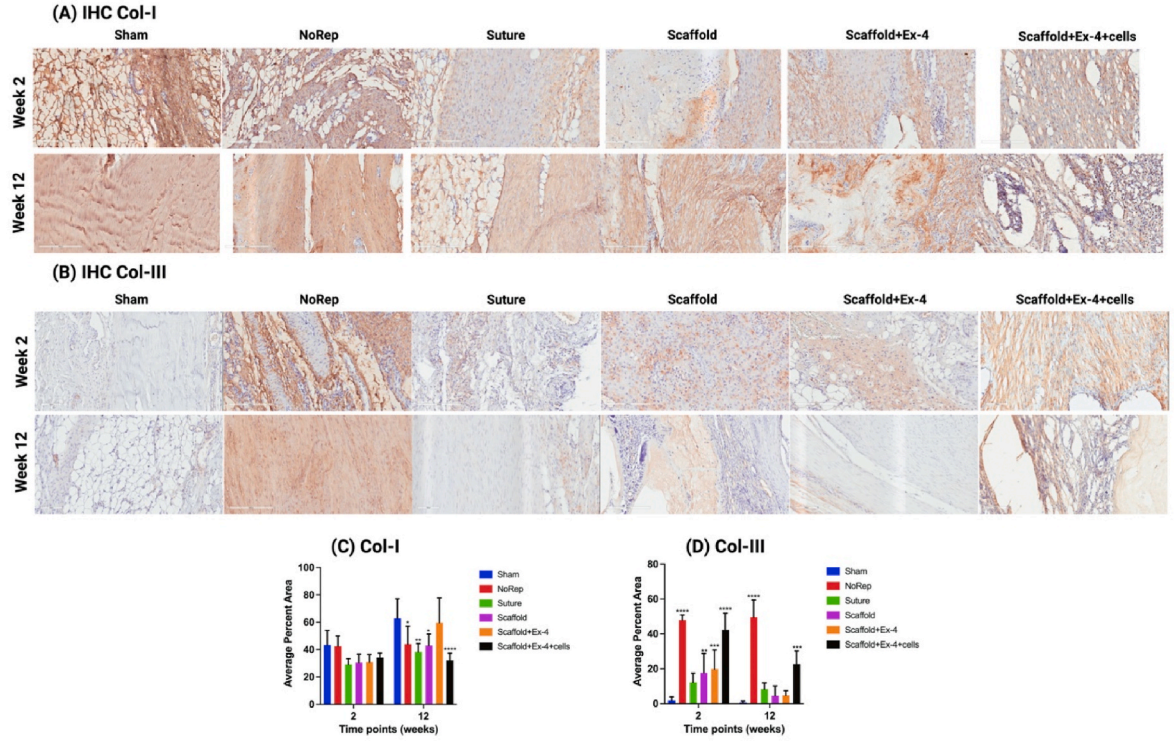

Fig. 7. All scaffold treatment groups demonstrated a significant elevation in Col-III protein expression at week 2 compared to sham which diminished at week 12 post-implantation. Rats treated with Scaffold/Ex-4 had Col-I comparable to the sham group. (A&C)Col-I protein expression was detected via IHC staining. All samples (n = 6) were evaluated using ImageJ. Data are presented as mean ± SD. * is $p < 0.05$; ** is $p < 0.01$; **** is $p < 0.0001$ compared to sham group. (B&D) Collagen-III protein expression detected via IHC staining. All samples (n = 6) were evaluated using ImageJ. Data are presented as mean ± SD. ** is $p < 0.01$; *** is $p < 0.001$; **** is $p < 0.0001$ compared to sham group. The scale bar is 200 μm.

3.17. Mechanical testing

To further demonstrate the tendon healing effect of implanted bioactive scaffolds, tensile mechanical testing was performed (Fig. 13). During the mechanical testing, all the native tendons failed by either skin slippage (30%) or calcaneus breakage (70%). At week 2 post-surgery, all repaired groups demonstrated tendon failure at the defect area; whereas they demonstrated tendon failure by calcaneus breakage. The structural mechanical properties of the tendon [6], including stiffness and maximum load, demonstrated no significant difference between the groups; whereas the intrinsic mechanical properties revealed differences between the groups. The elastic modulus of the sham group was significantly elevated compared to other groups at week 12. At both 2- and 12 weeks post-surgery, the sham group demonstrated a significant increase in ultimate stress. Interestingly, both suture and scaffold with Ex-4 groups exhibited significant increases in ultimate stress compared to the no-repair group (negative control).

4. Discussion

In this study, we successfully demonstrate the fabrication of a bioactive nanofiber matrix to deliver the peptide Ex-4 over 12 weeks while overcoming burst release issues. Blends of natural and synthetic polymers as well as semi-synthetic polymers have proven to be beneficial scaffold materials in tissue engineering due to their ability to mimic natural ECM structure and composition [2,10,11,15]. A wide range of scaffold fabrication techniques has been developed to meet the requirements of specific tissue structures as well as material physicochemical properties [17,18]. Fiber matrices with both micro and nanofibers have been a popular choice in soft-tissue regeneration [10,14,16]. Electrospun micro-nano fiber matrices of natural materials, synthetic materials, and their blends have been explored as scaffolds for tendon tissue engineering [10,14,16,19]. In the present study, we electrospun fiber matrices using an optimized 80:20 wt ratio of PCL and CA based on our prior publication [14]. Synthetic polyester PCL is an FDA-approved polymeric excipient for a variety of scaffolding and drug delivery applications [14,21,22]. Despite great mechanical compliance, PCL continues to face reduced cell-material interaction due to its hydrophobicity [14]. As a consequence, cells grown on PCL scaffolds often delaminate and fail to integrate with host tissue, resulting in suboptimal soft-tissue regeneration [57,58]. CA is another FDA-approved excipient used as a drug delivery matrix or in pharmaceutical preparations [14]. Electrospun CA fibers are loose, much like a cotton ball, without any mechanical integrity [2,16]. The electrospun PCL: CA matrices promote cell-material interaction without compromising the mechanical compliance needed for tendon repair and regeneration [14].

Electrospun fiber matrices, despite their excellent mimicry of native ECM structure, fail to provide bioactivity in the form of growth factors to modify the tissue healing response [13]. Efforts to deliver growth factors and other drugs using fiber matrices result in poor encapsulation efficiency and burst release of the drug in a very short period [24–26]. Many efforts to overcome such challenges – including coating fiber matrices with another barrier polymer layer, chemical tethering, and encapsulating drugs into secondary carriers before electrospinning – have had varying degrees of success and fabrication complexity [27]. More recently, inorganic nanotubes including carbon nanotubes and HNTs were used to carry drugs in their open lumens. In polymeric scaffolds where the ends of these tubes are closed, nanotubes serve as a drug depot that can reduce the burst effect and sustain release [28,29].

We successfully encapsulated Ex-4 in the open lumen of HNTs with an efficiency of 8.73% which is in agreement with literature-reported values ranging from 5 to 10% [31,32]. Inclusion of 2.5 wt % of Ex-4-carrying HNTs within fiber matrices did not significantly alter the fiber morphology, diameter, or matrix tensile properties as compared to

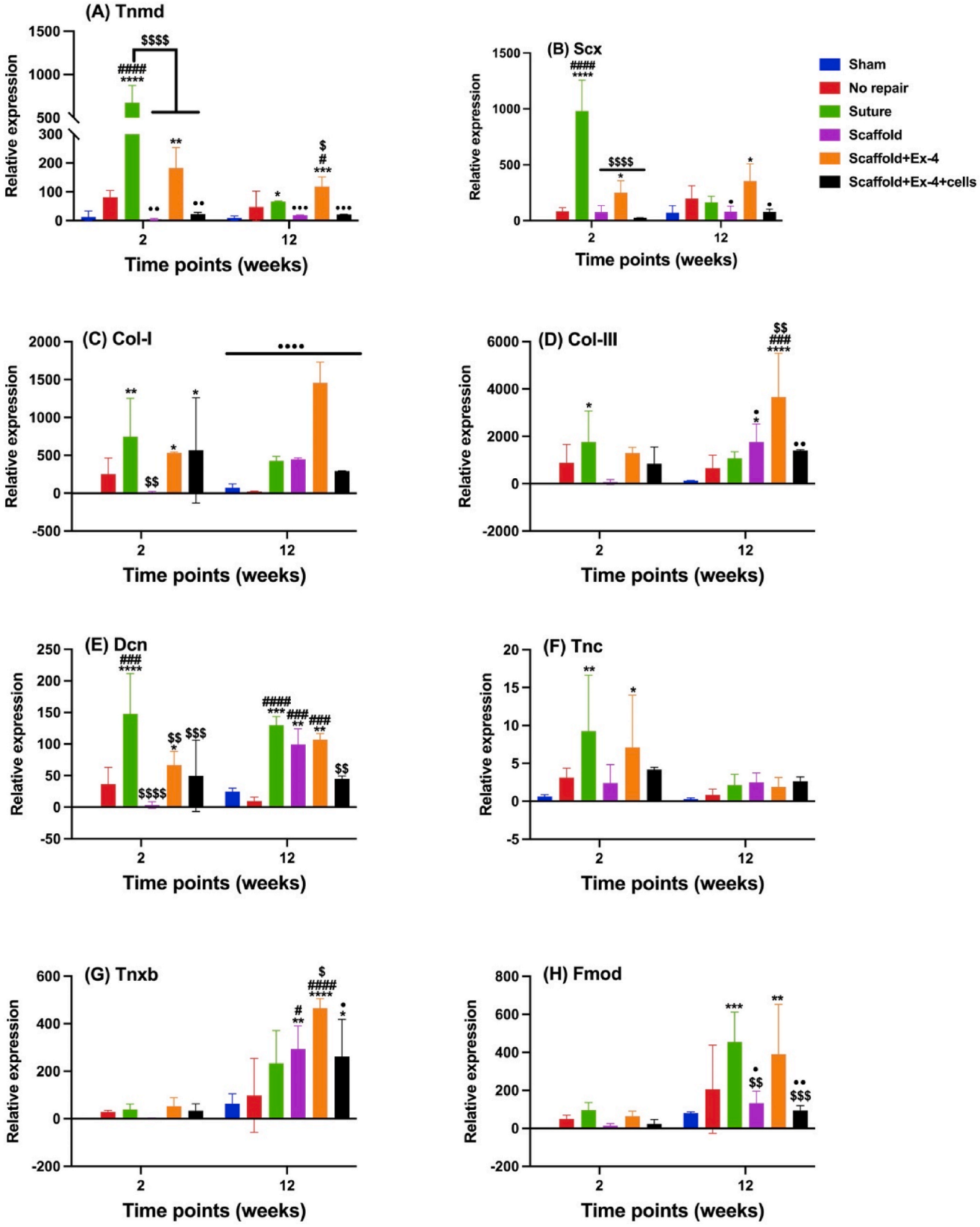

Fig. 8. Rats treated with suture or scaffold with Ex-4 demonstrated upregulation of tendon development-related genes compared to sham (control). The gene expression of (n = 3) in each group was quantified. * is $p < 0.05$; ** is $p < 0.01$; *** is $p < 0.001$; **** is $p < 0.0001$ compared to sham (control). # is $p < 0.05$; ### is $p < 0.001$; #### is $p < 0.0001$ compared to no repair group (negative control). $ is $p < 0.05$; $$ is $p < 0.01$; $$$ is $p < 0.001$; $$$$ is $p < 0.0001$ compared to suture (Positive control). • is $p < 0.05$; •• is $p < 0.01$; ••• is $p < 0.001$; •••• is $p < 0.0001$ compared to scaffold with Ex-4.

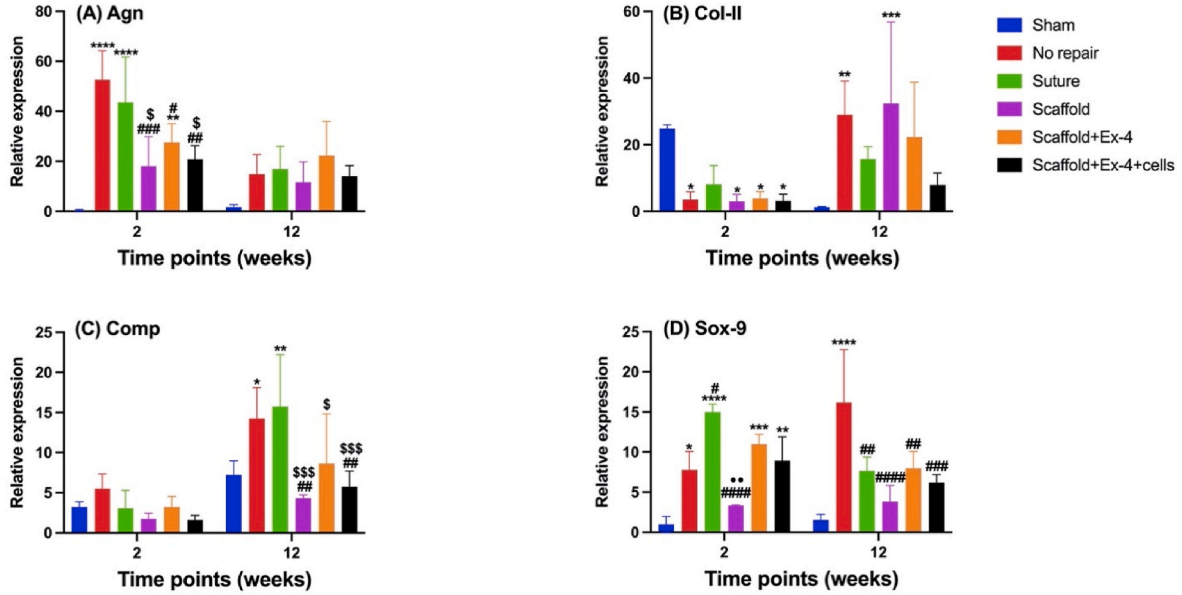

Fig. 9. Rats treated with scaffold with Ex-4 reduced the expression of chondrogenic-associated genes. The gene expression of (n = 3) in each group was quantified. * is $p < 0.05$; ** is $p < 0.01$; *** is $p < 0.001$; **** is $p < 0.0001$ compared to native (control). # is $p < 0.05$; ## is $p < 0.01$; ### is $p < 0.001$; #### is $p < 0.0001$ compared to no repair group (negative control). $ is $p < 0.05$; $$$ is $p < 0.001$ compared to suture (Positive control).

neat polymeric fiber matrices. In the composite fiber matrix, HNTs are aligned in the direction of the fibers as evidenced in fluorescent imaging (Fig. 2B). The lower HNT doping concentration and its homogenous distribution within the fibers potentially avoid phase separation and maintain matrix properties. The bead-free and randomly oriented electrospun fibers closely mimic the structure and diameter of collagen fibers in the tendon [59].

Drug loading by direct mixing with an electrospinning solution often results in poor encapsulation efficiency as a result of its preferential deposition on the fiber surface due to the applied electric field during the spinning process [25,26]. This may be an advantage for the poorly water-soluble drug in improving solubility as a result of enhanced surface area and lower drug crystallinity [11]. An approximately three-fold increase in the encapsulation efficiency of Ex-4 within the fiber matrix increased with the utilization of Ex-4-loaded HNTs as compared to direct drug mixing. Similar findings were also reported in the literature where secondary drug carriers were used in the scaffold system [29]. Such an approach also significantly reduced the burst release by approximately half and provided a sustained release of Ex-4 over an extended period as desired. In our system, utilization of HNTs-Ex-4 reduced the burst release from ~75% to ~40%.

In electrospun fiber matrices, the drug release is characterized by initial burst release followed by the diffusion/erosion-controlled secondary phase [26]. The burst release ranges from a few hours to three days based on the nature of the carrier polymer and the drug, and where the drug on the fiber surface will be leached out [26]. In our system, we also saw a similar burst release phase followed by a second phase where sustained drug release occurred via diffusion. The linear release profile post 1 day with our formulation demonstrated a zero-order release profile [26,60]. The Ex-4 release profiles from both matrices were found to fit well with the Higuchi and K–P models [60]. The diffusional exponent n value less than 0.5 is suggestive of Fickian diffusion where the drug diffuses out of the carrier from a higher concentration gradient to sink [60]. Overall, our approach enabled us to create a fiber matrix to release the drug at a constant rate over an extended period while reducing the burst effect. Thus our PCL-CA matrix with HNTs-Ex-4 extended the release of Ex-4 up to 12 weeks and may have the ability to modify tissue healing response at the most critical stages (inflammation and proliferation) of tendon healing [2].

The tenogenic factor Ex-4 is a long-lasting analog of glucagon-like peptide-1, but its half-life is short (60–90 min) [42,61]. For tendon tissue regeneration, it is essential to release Ex-4 at the site of injury by encapsulating it within the matrix used for reconstruction and ensuring the retainment of its bioactivity. A series of in vitro tissue culture experiments conducted using hMSCs confirm the fiber matrix bioactivity by inducing their tenogenic differentiation. In our prior work, the optimal dose of Ex-4 to induce hMSCs into the tenogenic lineage was found to be 20 nM [40]. The designed fiber matrix and released Ex-4 mirrored the effects of continuous 20 nM Ex-4 treatment (positive control) in terms of cell attachment, proliferation, and viability.

The efficacy of the bioactive matrix in promoting tenogenic differentiation of hMSCs was evaluated by quantifying ECM components such as collagen and proteoglycan as well as tendon-specific genes. Type I collagen is predominant in native tendons [1,2,62] while proteoglycan, though a minor ECM component, plays a critical role in maintaining the mechanical stability of the collagen fibrils through resisting high compressive and tensile forces [1,59]. Similar levels of collagen and s-GAG deposition under the continuous 20 nM Ex-4 treatment and the encapsulated Ex-4 confirm the successful design of the matrix in terms of ECM mimicry and delivery of optimal dose [2,14]. However, we observed noticeable changes in tenogenic gene expression and timing of peak expression between Ex-4-loaded HNT and the Ex-4 continuous treatment. Such an effect may come from many sources including the contributions of matrix architecture [14], the presence of HNTs [29], variations in Ex-4 exposure, and cell cycle, to name a few [63]. For example, fiber matrices with HNTs-Ex-4 followed a favorable expression where Col-I/Col-III increased, reflecting the high expression of Col-I, which is vital for tendon healing and development [1]. The early expression of Scx and Tnmd by hMSCs on the fiber matrices with HNTs-Ex-4 proved the vital role of HNT to preserve Ex-4 bioactivity. The designed bioactive nanofiber matrix with Ex-4 successfully cued the seeded hMSCs toward tenogenic differentiation. Our finding illustrated the vital role of HNT encapsulation to sustain Ex-4 release while maintaining its bioactivity, which accelerates cellular proliferation and differentiation.

There are currently no known treatments that provide scarless tendon healing; therefore, new treatment modalities are essential to provide better tendon healing and completely restore tendon

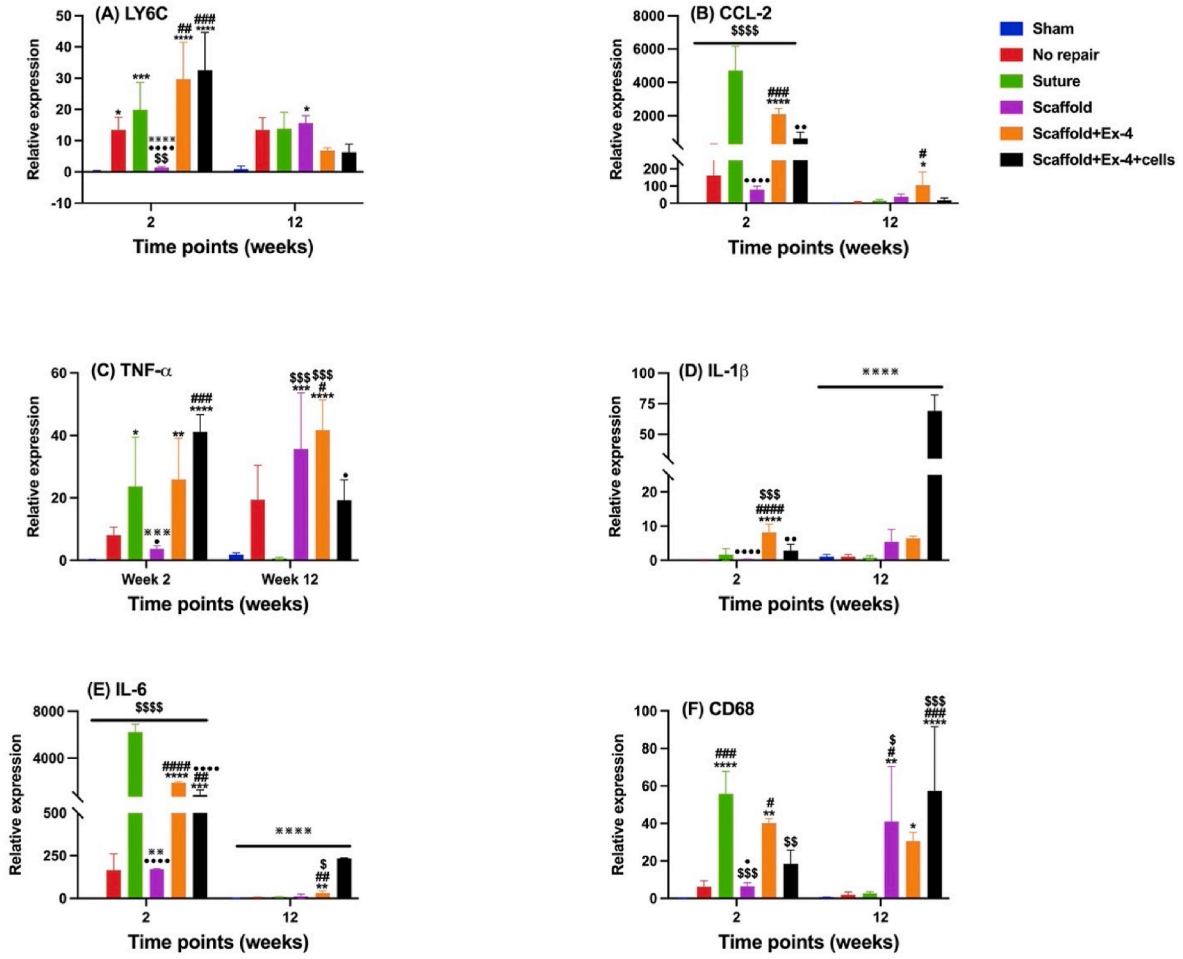

Fig. 10. Pro-inflammatory gene expression was elevated at week 2 post-surgery for suture, scaffold with Ex-4 and scaffold with Ex-4 and rMSCs, and some genes (CD68 and IL-6) remained elevated for scaffold with Ex-4 and scaffold with Ex-4 and rMSCs. Relative gene expression of pro-inflammatory cytokines. The gene expression of (n = 3) in each group was quantified. * is $p < 0.05$; ** is $p < 0.01$; *** is $p < 0.001$; **** is $p < 0.0001$ compared to native (control). # is $p < 0.05$; ## is $p < 0.01$; ### is $p < 0.001$; #### is $p < 0.0001$ compared to no repair group (negative control). $ is $p < 0.05$; $$ is $p < 0.01$; $$$ is $p < 0.001$; $$$$ is $p < 0.0001$ compared to suture (Positive control). • is $p < 0.05$; •• is $p < 0.01$; •••• is $p < 0.0001$ compared to scaffold with Ex-4. ⁎⁎ is $p < 0.01$; ⁎⁎⁎ is $p < 0.001$; ⁎⁎⁎⁎ is $p < 0.0001$ compared to scaffold with Ex-4 and rMSCs.

functionality [64]. The ultimate goal of the present study is to assess the feasibility of the fabricated PCL-CA scaffold loaded with halloysite nanotube-encapsulated exendin-4 (HNT-Ex-4) to promote tendon healing and regeneration. Previously, we investigated the efficacy of Ex-4 to cue hMSCs toward tenogenesis in vitro. The results demonstrated that Ex-4 promoted tenogenic differentiation of hMSCs [50]. To further our investigation, a rat tendon repair model was used to evaluate the performance of the scaffold in an in vivo environment, which helps with understanding the cellular and tissue healing level in a living organism [65]. Herein, Achilles tendon transection was performed, and the scaffold was implanted as a wrap and fixed with a suture. The plantar tendon was removed to produce a model similar to human anatomy [66]. We successfully provided tendon healing with histological, functional, molecular, and mechanical restoration equivalent to the suture group (positive control) and significantly better than the no-repair group (negative control).

Several researchers have investigated the benefits of MSCs in tendon tissue engineering due to their ability to reduce inflammatory cell infiltration, enhance collagen organization, and reduce ECM disorganization [67–70]. In this study, we tracked MSCs to study how Ex-4 and HNTs affect cell-scaffold interactions. Before surgery, rMSCs were extracted, fluorescently labeled, seeded on the scaffold, and allowed to attach for 24 h. We were able to trace the labeled cells in vitro and in vivo for up to 12 weeks. However, the number of traced cells in vivo was low at week 12, potentially due to host reaction or cellular division of the donor cells within the host.

The polymeric encapsulation of Ex-4 successfully restored Ex-4 bioactivity for up to 7 or 14 days for scaffold with Ex-4 and scaffold with Ex-4 and MSC groups, respectively, which is the highest among previously reported systems [42,71,72]. The systemic detection of Ex-4 might be attributed to the burst release which was extended up to 14 days when MSCs were seeded. The systemic immunological effect was addressed by tracking the serum level of IL-6 and IL-10 for the first two weeks. The anti-inflammatory effects of Ex-4 only or in combination with MSCs were confirmed by diminishing IL-6 levels followed by IL-10 elevation which came in agreement with previous reports [73–75].

Different aspects were considered in the healing assessment. The gross morphology of Achilles tendons treated with suture or scaffold with Ex-4 exhibited similar tendon length to the native tendon. Furthermore, all groups exhibited higher cross-sectional area than native tendons at week 2, but this became smaller at week 12. Prior studies revealed that the increased length of the Achilles tendon is associated with poor healing, while a high cross-sectioned area is indicative of tendon callus formation [76–79]. All polymeric scaffolds remained in place at the surgical location.

The histomorphometric analysis revealed an elevation in total

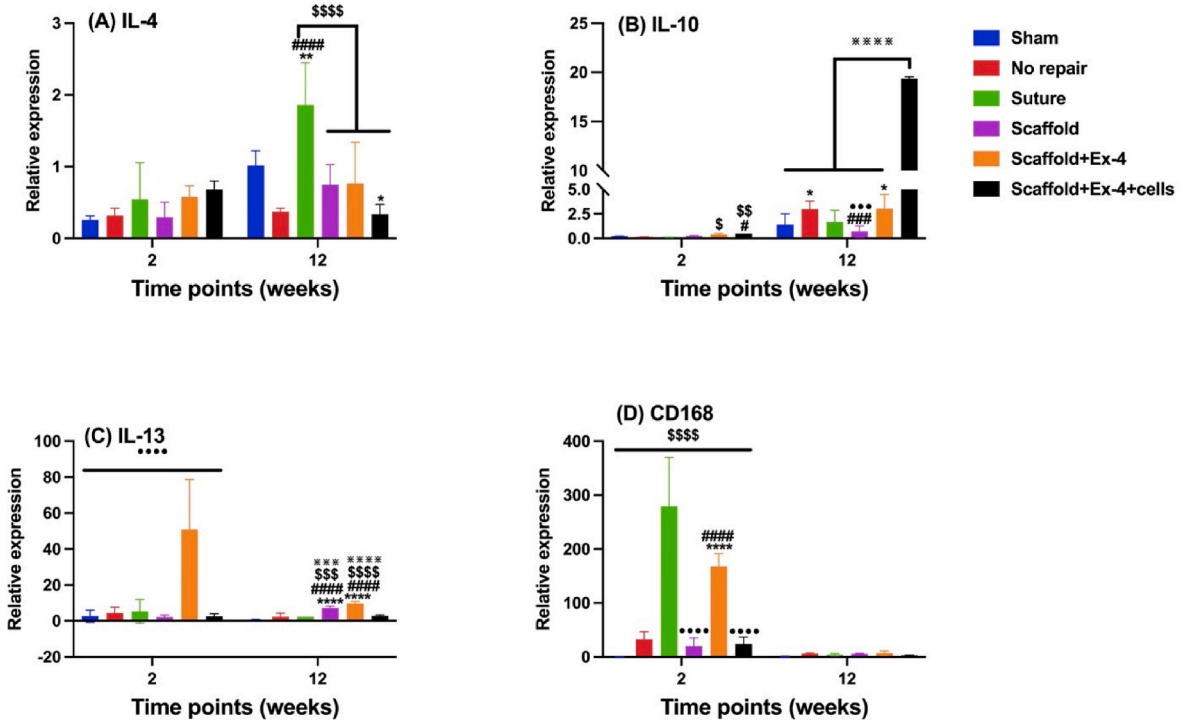

Fig. 11. Relative gene expression of anti-inflammatory cytokines at weeks 2 & 12 post-surgery. The gene expression of (n = 3) in each group was quantified. * is $p < 0.05$; ** is $p < 0.01$; *** is $p < 0.001$; **** is $p < 0.0001$ compared to native (control). # is $p < 0.05$; ## is $p < 0.01$; ### is $p < 0.001$; #### is $p < 0.0001$ compared to no repair group (negative control). $ is $p < 0.05$; $$ is $p < 0.01$; $$$ is $p < 0.001$; $$$$ is $p < 0.0001$ compared to suture (Positive control). • is $p < 0.05$; •• is $p < 0.01$; •••• is $p < 0.0001$ compared to scaffold with Ex-4. ⁎⁎ is $p < 0.01$; ⁎⁎⁎ is $p < 0.001$; ⁎⁎⁎⁎ is $p < 0.0001$ compared to scaffold with Ex-4 and rMSCs.

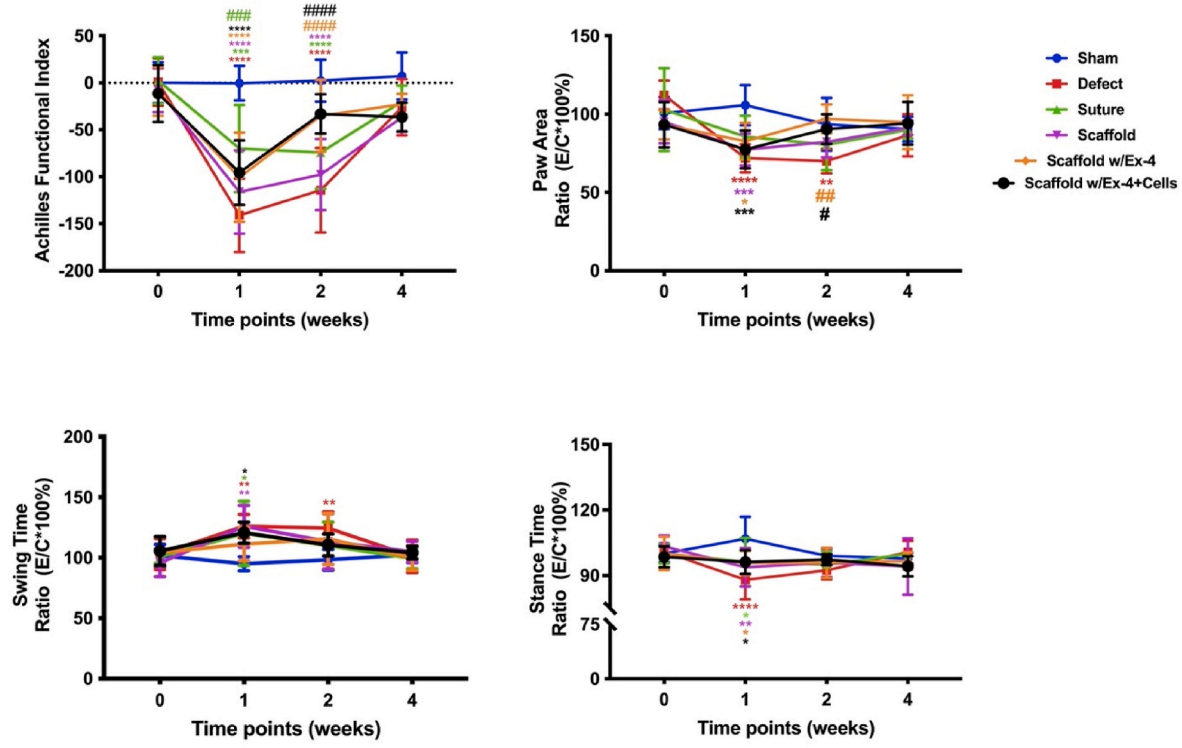

Fig. 12. Rats treated with scaffold loaded HNT-Ex-4, scaffold seeded with rMSCs, and Suture repair demonstrated better functional recovery from full-thickness Achilles tendon transection. The assessment was performed at different time points using DigiGait analysis. (A) Achilles functional index (AFI). (B) Paw area which represents the size of the paw during the stance phase. (C) Swing time. (D) Stance time. The results (n = 6–8 per group for each timepoint) are shown as mean ± SD. * is $p < 0.05$, ** is $p < 0.01$, *** is $p < 0.001$, and **** is $p < 0.0001$ compared to sham. # is $p < 0.05$, ## is $p < 0.01$, ### is $p < 0.001$, and #### is $p < 0.0001$ compared to no repair group.

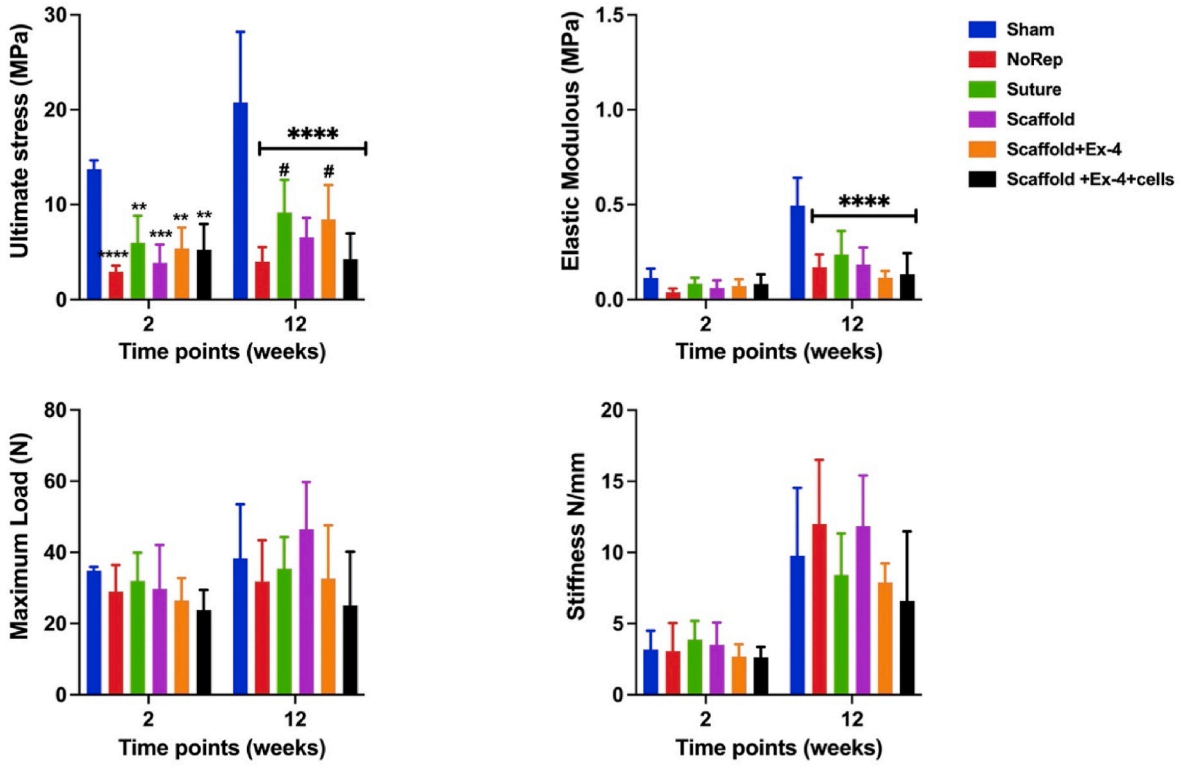

Fig. 13. Rat treated with suture or scaffold with Ex-4 demonstrated significantly high ultimate stress compared to no repair group (negative control). Mechanical testing of (n = 6) for each group per timepoint was conducted using the uniaxial tensile test. ** is $p < 0.01$; *** is $p < 0.001$; **** is $p < 0.0001$ compared to the sham group. # is $p < 0.05$ compared to the no repair group (negative control).

scoring of histological assessment, which was mainly attributed to cellularity, inflammation, and rounded nuclei. Cellular infiltration was evident within the scaffolds which indicates that the structural properties of the scaffold aid cellular infiltration and vascularization [2,80]. All scaffold treatment groups demonstrated a significant increase in inflammation which was recognized as multinucleated giant cells (MNGC) and macrophages. MNGCs usually became evident 15 days post-implantation [81]. It is suggested that MNGCs are formed by the initial fusion of aggregated macrophages in response to the implantation. The main role of these cells to aid biomaterial degradation or integration remains debatable. These cells can express both pro-inflammatory (M1-MNGCs) and anti-inflammatory (M2-MNGCs) molecules within the implantation location [82]. Udeabor et al. reported that the accumulation of MNGCs along with increased vascularization is correlated to biomaterial degradation. However, our study demonstrated that MNGC accumulation and increased vascularization were associated with slow degradation and high expression of pro-inflammatory (CD-68, TNF-α, and IL-1β) and anti-inflammatory (IL-4, IL-10, and IL-13) markers at later timepoints. It has been reported that pro-inflammatory macrophages and MNGCs develop distinct properties by enhancing the expression of important growth factors and cytokines such as vascular endothelial growth factor (VEGF), which is important for angiogenesis [81,83,84]. This evidence suggested that the tendon healing process was underway, but further investigation is necessary to confirm this process.

The histological examination using Masson's trichrome staining depicted the collagen maturation stage in which blue staining is associated with neo-collagen formation while red staining is associated with mature collagen [48,64,85]. Similar to the previous finding, blue staining was evident in week 2, indicating that neo-collagen formation occurs after the massive disruption induced to the collagen fibers after surgery. This effect was significantly reduced at week 12 in rats treated with scaffold + Ex-4 or scaffold + Ex-4+rMSCs. Likewise, red staining was comparable to sham and suture when rats were treated with scaffold + Ex-4. This confirmed that Ex-4 alone or in combination with rMSCs is the key contributor to tendon healing.

Immunohistochemistry aimed to detect the protein level of Col-I and Col-III. The ideal healing of the tendon after injury includes a dramatic increase in Col-III formation, which shifted to an increase in Col-I later [2,86]. Our results followed the mechanism of healing in which Col-III formation was remarkably increased at week 2 and diminished by week 12, associated with excessive elevation of Col-I expression.

To further assess tendon healing, we investigated ECM-related and tendon-specific gene expression. Tendon-specific genes (Tnmd, Scx, Col-I, and Col-III) were more upregulated in rats treated with scaffold + Ex-4 than in the other groups, which strongly suggests tendon healing. Furthermore, the high expression of Fmod was evident in rats treated with suture and scaffold + Ex-4 as well. High expression of Fmod was previously reported to be associated with tendon healing [51]. A mouse model with Fmod deficiency demonstrated decreased diameter of collagen fibrils as well as heterotopic ossification [87]. The reciprocal gene expression of Tnc and Tnxb was remarkably evident for rats treated with scaffold + Ex-4. The early expression of Tnc was usually associated with the late expression of Tnxb, and both genes are highly expressed in tendons [88–91]. The high expression of Scx along with low Sox-9 expression indicated tendon regeneration [64]. Overall, tendon-related gene expression was upregulated in rats treated with scaffold + Ex-4, suggesting that scaffolds + Ex-4 promote tendon healing.

Tendon healing is divided into three distinct phases: inflammation, proliferation, and remodeling [86,92]. The alteration of various pro- and anti-inflammatory cytokines is critical to improving tendon healing during the healing process [85]. Similar to previous reports [85,92,93], the expression of pro-inflammatory cytokines (TNF- α, IL-1β, and IL-6) was evident at week two, but IL-1β and IL-6 were reduced by week 12 post-implantation. Anti-inflammatory cytokine expression (IL-4, IL-10, and IL-13) was evident in week 12, which is associated with tendon

healing and regeneration [94]. Klatte-Schulz et al. reported that acute rupture tendon is associated with high expression of IL-6, IL-10, and CD-68 [95]. Aktas et al. reported that TNF-α induced PGE_2 resulting in increased expression of IL-6 and anti-inflammatory cytokines IL-4 and IL-10 [96]. These inflammatory cytokines play critical roles in tendon healing; however, their exact role in tendon development and healing remains unclear [94].

Heterotopic ossification (HO) is a common complication characterized by tendon repair, which is associated with elevated chondrogenic and osteogenic gene expression [97]. Pathological formation of endochondral or intramembranous bone in soft tissue usually happens after injury [98,99]. It is associated with collagen type II, proteoglycan elevation, as well as rounded cellular morphology. Different studies have reported the upregulation of inflammatory cytokines such as IL-1β, IL-6, and TNF-α during HO as causation [100,101], while other reports attributed their upregulation to erroneous fibroblast differentiation [102,103]. Our study revealed that HO is not associated with inflammatory cytokine upregulation. Rats left without treatment (no repair group) demonstrated the highest expression of chondrogenic markers (Sox-9, Comp, and Col-II) with the lowest expression of inflammatory markers (IL-1β, IL-6, and TNF-α). Histomorphometric analysis and safranin-O staining revealed that the highest chondrification was evident in no repair as well as scaffold groups. Interestingly, rats treated with scaffold + Ex-4 demonstrated lower chondrification compared to the suture group, suggesting that Ex-4 promotes tendon healing. The osteogenic markers (IBSP, ALP, and SMAD-1) expression was upregulated when rats were treated with scaffold + Ex-4+rMSCs. Different reports revealed no effect of MSCs on tendon healing [104,105].

The functional outcome of healed tendons was assessed by performing mechanical testing and DigiGait analysis. Mechanical properties are critical indicators for recovered motor ability [48]. The present work has demonstrated that rats treated with scaffold + HNT-Ex-4 improve mechanical properties, in which ultimate stress was significantly increased compared to negative control (no repair group) 12 weeks post-implantation. DigiGait analysis is another vital assessment toward functional recovery. Achilles' functional index (AFI) is a sensitive parameter that detects any functional deficit. It exhibits normal function for the sham group while other groups subjected to Achilles transection demonstrated impaired function which gradually improved [66]. Previous reports demonstrated that AFI gradual recovery occurred two weeks post-surgery [3,66,106]. Similar to previous reports, all groups gradually returned to the normal range 2 weeks post-implantation. Interestingly, rats treated with scaffold + Ex-4 or scaffold + Ex-4+rMSCs demonstrated functional recovery comparable to the sham group and significantly better than no repair groups. Other parameters have been considered in the functional assessment such as paw area ratio, swing time ratio, and stance time ratio which also further confirmed the effect of Ex-4 toward tendon functional recovery. These findings suggest that Ex-4 enhances tendon healing and regeneration.

To the best of our knowledge, no previous work has studied the role of Ex-4 in vivo to promote tendon healing and regeneration. However, the present study demonstrated some limitations. The Achilles tendon defect was induced by a clean transection which is different than how it occurs in reality; clinically, Achilles tendon rupture does not happen as a clean cut. Future research should implement an animal model that creates a tendon rupture with more torn edges [66].

5. Conclusion

The present study has investigated thoroughly the efficacy of Ex-4 delivered in a polymeric matrix to achieve better tendon healing in a rat model. Scaffolds loaded with Ex-4 have successfully promoted tendon healing with better collagen deposition, gene upregulation, functional recovery, and mechanical properties. The ability of our blended nanofiber matrix to provide sustained delivery of the small-molecule Ex-4 and induce desirable tenogenic responses of hMSCs supports their potential for tendon repair and regeneration and as a model for future tissue-engineering strategies. Collectively, scaffolds loaded with Ex-4 demonstrated a great contribution to tendon tissue engineering, which could be a potential strategy in future clinical applications.

Ethics approval

It is a research manuscript and human subjects were not involved. Therefore no "ethics approval and consent" needed.

CRediT authorship contribution statement

Sama Abdulmalik: Data curation, Formal analysis, Methodology, Writing – review & editing. **Jack Gallo:** Methodology, and review, Writing – review & editing. **Jonathan Nip:** Methodology, and review, Writing – review & editing. **Sara Katebifar:** Methodology, and review, Writing – review & editing. **Michael Arul:** Methodology, and review, Writing – review & editing. **Amir Lebaschi:** Methodology, and review, Writing – review & editing. **Lucas N. Munch:** Methodology, and review, Writing – review & editing. **Jenna M. Bartly:** Methodology, and review, Writing – review & editing. **Shilpa Choudhary:** Methodology, review & editing, Writing – review & editing. **Ivo Kalajzic:** Methodology, review & editing, Writing – review & editing. **Yeshavanth Kumar Banasavadi-Siddegowdae:** Methodology, review & editing, Writing – review & editing. **Syam P. Nukavarapu:** Methodology, review & editing, Writing – review & editing. **Sangamesh G. Kumbar:** Conceptualization, Data curation, Formal analysis, Methodology, Project administration, Supervision, Funding acquisition, Writing – review & editing.

Declaration of competing interest

All authors have been involved in writing of the review article and each of the authors has read and concurs with the content in the review article. All authors and co-authors accept the submission of the review article without any conflict of interest.

Acknowledgment

Authors acknowledge the funding support was provided by the National Institute of Biomedical Imaging and Bioengineering of the National Institutes of Health (#R01EB020640, #R01EB030060, #R56NS122753 and R01 AR078908-01); the Assistant Secretary of Defense for Health Affairs through the Peer Reviewed Orthopaedic Research Program [#W81XWH-20-1-0321]. Also, the author acknowledges the educational scholarship sponsored by The Minster of Education, Riyadh, Kingdom of Saudi Arabia, in coordination with the Saudi Arabian Cultural Mission in VA, USA. The authors thank Soliman Alhudaithy for his assistance with matrix mechanical testing. The authors also thank Christopher Bonin and Geneva Hargis for manuscript edits. The authors thank Dr. Sanja Novak and Dr. Zana Kalajzic for their help with PCR and histology evaluation.

Appendix A. Supplementary data

Supplementary data to this article can be found online at https://doi.org/10.1016/j.bioactmat.2023.01.013.

References

[1] J.G. Snedeker, J. Foolen, Tendon injury and repair–A perspective on the basic mechanisms of tendon disease and future clinical therapy, Acta Biomater. 63 (2017) 18–36.
[2] A.V. Vasiliadis, K. Katakalos, The role of scaffolds in tendon tissue engineering, J. Funct. Biomater. 11 (4) (2020) 78.

[3] W.R. Webb, et al., The application of poly (3-hydroxybutyrate-co-3-hydroxyhexanoate) scaffolds for tendon repair in the rat model, Biomaterials 34 (28) (2013) 6683–6694.
[4] G. Yang, B.B. Rothrauff, R.S. Tuan, Tendon and ligament regeneration and repair: clinical relevance and developmental paradigm, Birth Defects Res., Part C 99 (3) (2013) 203–222.
[5] J. Chen, et al., Scaffolds for tendon and ligament repair: review of the efficacy of commercial products, Expet Rev. Med. Dev. 6 (1) (2009) 61–73.
[6] P.P.Y. Lui, Stem cell technology for tendon regeneration: current status, challenges, and future research directions, Stem Cell. Clon Adv. Appl. 8 (2015) 163.
[7] K. Otabe, et al., Transcription factor Mohawk controls tenogenic differentiation of bone marrow mesenchymal stem cells in vitro and in vivo, J. Orthop. Res. 33 (1) (2015) 1–8.
[8] K. Howell, et al., Novel model of tendon regeneration reveals distinct cell mechanisms underlying regenerative and fibrotic tendon healing, Sci. Rep. 7 (1) (2017) 1–14.
[9] G. Nourissat, F. Berenbaum, D. Duprez, Tendon injury: from biology to tendon repair, Nat. Rev. Rheumatol. 11 (4) (2015) 223.
[10] N. Narayanan, et al., Polymeric electrospinning for musculoskeletal regenerative engineering, Regener. Eng. Transl. Med. 2 (2) (2016) 69–84.
[11] S. Kumbar, et al., Electrospun nanofiber scaffolds: engineering soft tissues, Biomed. Mater. 3 (3) (2008), 034002.
[12] R. James, et al., Tendon tissue engineering: adipose-derived stem cell and GDF-5 mediated regeneration using electrospun matrix systems, Biomed. Mater. 6 (2) (2011), 025011.
[13] C. Hu, et al., Long-term drug release from electrospun fibers for in vivo inflammation prevention in the prevention of peritendinous adhesions, Acta Biomater. 9 (7) (2013) 7381–7388.
[14] D.M. Ramos, et al., Insulin immobilized PCL-cellulose acetate micro-nanostructured fibrous scaffolds for tendon tissue engineering, Polym. Adv. Technol. 30 (5) (2019) 1205–1215.
[15] H. Yuan, et al., Collagen and chondroitin sulfate functionalized bioinspired fibers for tendon tissue engineering application, Int. J. Biol. Macromol. 170 (2021) 248–260.
[16] S. Liu, et al., Tendon healing and anti-adhesion properties of electrospun fibrous membranes containing bFGF loaded nanoparticles, Biomaterials 34 (19) (2013) 4690–4701.
[17] S.K. Czaplewski, et al., Tenogenic differentiation of human induced pluripotent stem cell-derived mesenchymal stem cells dictated by properties of braided submicron fibrous scaffolds, Biomaterials 35 (25) (2014) 6907–6917.
[18] R. James, et al., Electrospun nanofibrous scaffolds for engineering soft connective tissues, in: Biomedical Nanotechnology, Springer, 2011, pp. 243–258.
[19] X. Xie, et al., Electrospinning nanofiber scaffolds for soft and hard tissue regeneration, J. Mater. Sci. Technol.59 (2020) 243–261.
[20] S.G. Kumbar, M.D. Harmon, Composite Fibers and Matrices Thereof, Google Patents, 2018.
[21] K. Ghosal, et al., Structural and surface compatibility study of modified electrospun poly (ε-caprolactone)(PCL) composites for skin tissue engineering, AAPS PharmSciTech 18 (1) (2017) 72–81.
[22] S. Stratton, et al., Bioactive polymeric scaffolds for tissue engineering, Bioact. Mater. 1 (2) (2016) 93–108.
[23] X. Hu, et al., Electrospinning of polymeric nanofibers for drug delivery applications, J. Contr. Release 185 (2014) 12–21.
[24] J. Xue, et al., Drug loaded homogeneous electrospun PCL/gelatin hybrid nanofiber structures for anti-infective tissue regeneration membranes, Biomaterials 35 (34) (2014) 9395–9405.
[25] S.M. Kamath, et al., Fabrication of tri-layered electrospun polycaprolactone mats with improved sustained drug release profile, Sci. Rep. 10 (1) (2020) 1–13.
[26] N. Kamaly, et al., Degradable controlled-release polymers and polymeric nanoparticles: mechanisms of controlling drug release, Chem. Rev. 116 (4) (2016) 2602–2663.
[27] Z. Wang, et al., Novel biomaterial strategies for controlled growth factor delivery for biomedical applications, NPG Asia Mater. 9 (10) (2017) e435-e435.
[28] O.S. Manoukian, et al., Biopolymer-nanotube nerve guidance conduit drug delivery for peripheral nerve regeneration: in vivo structural and functional assessment, Bioact. Mater. 6 (9) (2021) 2881–2893.
[29] O.S. Manoukian, et al., Aligned microchannel polymer-nanotube composites for peripheral nerve regeneration: small molecule drug delivery, J. Contr. Release 296 (2019) 54–67.
[30] J. Xue, et al., Electrospun microfiber membranes embedded with drug-loaded clay nanotubes for sustained antimicrobial protection, ACS Nano 9 (2) (2015) 1600–1612.
[31] Y.M. Lvov, M.M. DeVilliers, R.F. Fakhrullin, The application of halloysite tubule nanoclay in drug delivery, Expet Opin. Drug Deliv. 13 (7) (2016) 977–986.
[32] Y. Lvov, et al., Halloysite clay nanotubes for loading and sustained release of functional compounds, Adv. Mater. 28 (6) (2016) 1227–1250.
[33] T. Tu, et al., Tendon ECM modified bioactive electrospun fibers promote MSC tenogenic differentiation and tendon regeneration, Appl. Mater. Today 18 (2020), 100495.
[34] C.K. Kuo, R.S. Tuan, Mechanoactive tenogenic differentiation of human mesenchymal stem cells, Tissue Eng. 14 (10) (2008) 1615–1627.
[35] T.K. Teh, S.-L. Toh, J.C. Goh, Aligned fibrous scaffolds for enhanced mechanoresponse and tenogenesis of mesenchymal stem cells, Tissue Eng. 19 (11–12) (2013) 1360–1372.
[36] T.L. Popielarczyk, A.S. Nain, J.G. Barrett, Aligned nanofiber topography directs the tenogenic differentiation of mesenchymal stem cells, Appl. Sci. 7 (1) (2017) 59.
[37] J.M. Banks, et al., The combined effects of matrix stiffness and growth factor immobilization on the bioactivity and differentiation capabilities of adipose-derived stem cells, Biomaterials 35 (32) (2014) 8951–8959.
[38] A.I. Gonçalves, et al., Understanding the role of growth factors in modulating stem cell tenogenesis, PLoS One 8 (12) (2013), e83734.
[39] T.-C. Ho, et al., PEDF-derived peptide promotes tendon regeneration through its mitogenic effect on tendon stem/progenitor cells, Stem Cell Res. Ther. 10 (1) (2019) 1–15.
[40] S. Abdulmalik, et al., The Glucagon-like Peptide 1 Receptor Agonist Exendin-4 Induces Tenogenesis in Human Mesenchymal Stem Cells, Differentiation, 2021.
[41] F. Tong, Preparation of exenatide-loaded linear poly (ethylene glycol)-brush poly (l-lysine) block copolymer: potential implications on diabetic nephropathy, Int. J. Nanomed. 12 (2017) 4663.
[42] W. Chen, et al., Long-acting release formulation of exendin-4 based on biomimetic mineralization for type 2 diabetes therapy, ACS Nano 11 (5) (2017) 5062–5069.
[43] M.S. Peach, et al., Polyphosphazene functionalized polyester fiber matrices for tendon tissue engineering: in vitro evaluation with human mesenchymal stem cells, Biomed. Mater. 7 (4) (2012), 045016.
[44] S.B. Orr, et al., Aligned multilayered electrospun scaffolds for rotator cuff tendon tissue engineering, Acta Biomater. 24 (2015) 117–126.
[45] J.S. Mort, P.J. Roughley, Measurement of glycosaminoglycan release from cartilage explants, in: Arthritis Research, Springer, 2007, pp. 201–209.
[46] W. Kafienah, T.J. Sims, Biochemical methods for the analysis of tissue-engineered cartilage, in: Biopolymer Methods in Tissue Engineering, Springer, 2004, pp. 217–229.
[47] L. Zhang, C. Chan, Isolation and enrichment of rat mesenchymal stem cells (MSCs) and separation of single-colony derived MSCs, JoVE (37) (2010) e1852.
[48] J. Sun, et al., Controlled release of collagen-binding SDF-1α from the collagen scaffold promoted tendon regeneration in a rat Achilles tendon defect model, Biomaterials 162 (2018) 22–33.
[49] N.A. Dyment, et al., High-throughput, multi-image cryohistology of mineralized tissues, JoVE (115) (2016), e54468.
[50] S. Abdulmalik, et al., The glucagon-like peptide 1 receptor agonist Exendin-4 induces tenogenesis in human mesenchymal stem cells, Differentiation 120 (2021) 1–9.
[51] H. Suzuki, et al., Gene targeting of the transcription factor Mohawk in rats causes heterotopic ossification of Achilles tendon via failed tenogenesis, Proc. Natl. Acad. Sci. USA 113 (28) (2016) 7840–7845.
[52] K.B. Sugg, et al., Changes in macrophage phenotype and induction of epithelial-to-mesenchymal transition genes following acute Achilles tenotomy and repair, J. Orthop. Res. 32 (7) (2014) 944–951.
[53] A. Peinnequin, et al., Rat pro-inflammatory cytokine and cytokine related mRNA quantification by real-time polymerase chain reaction using SYBR green, BMC Immunol. 5 (1) (2004) 1–10.
[54] R.T. De Silva, et al., Drug-loaded halloysite nanotube-reinforced electrospun alginate-based nanofibrous scaffolds with sustained antimicrobial protection, ACS Appl. Mater. Interfaces 10 (40) (2018) 33913–33922.
[55] S.G. Kumbar, et al., Electrospun poly (lactic acid-co-glycolic acid) scaffolds for skin tissue engineering, Biomaterials 29 (30) (2008) 4100–4107.
[56] R. Gouda, H. Baishya, Z. Qing, Application of mathematical models in drug release kinetics of carbidopa and levodopa ER tablets, J. Dev. Drugs 6 (2017) 1–8, 02.
[57] P. Bhaskar, et al., Cell response to sterilized electrospun poly (ε-caprolactone) scaffolds to aid tendon regeneration in vivo, J. Biomed. Mater. Res. 105 (2) (2017) 389–397.
[58] M. Mozafari, et al., Synthesis and characterisation of highly interconnected porous poly (ε-caprolactone)-collagen scaffolds: a therapeutic design to facilitate tendon regeneration, Mater. Technol. 33 (1) (2018) 29–37.
[59] P. Kannus, Structure of the tendon connective tissue, Scand. J. Med. Sci. Sports 10 (6) (2000) 312–320.
[60] O.S. Manoukian, et al., Biodegradable polymeric injectable implants for long-term delivery of contraceptive drugs, J. Appl. Polym. Sci. 135 (14) (2018), 46068.
[61] Y. Li, et al., Pharmacokinetics of Exenatide in nonhuman primates following its administration in the form of sustained-release PT320 and Bydureon, Sci. Rep. 9 (1) (2019) 1–10.
[62] R. James, et al., Tendon: biology, biomechanics, repair, growth factors, and evolving treatment options, J. Hand Surg. 33 (1) (2008) 102–112.
[63] T.K. MacLachlan, et al., BRCA1 effects on the cell cycle and the DNA damage response are linked to altered gene expression, J. Biol. Chem. 275 (4) (2000) 2777–2785.
[64] S. Korntner, et al., A high-glucose diet affects Achilles tendon healing in rats, Sci. Rep. 7 (1) (2017) 1–12.
[65] M. Hast, A. Zuskov, L. Soslowsky, The role of animal models in tendon research, Bone & Joint Res. 3 (6) (2014) 193–202.
[66] G.A. Murrell, et al., The Achilles functional index, J. Orthop. Res. 10 (3) (1992) 398–404.
[67] R. Costa-Almeida, I. Calejo, M.E. Gomes, Mesenchymal stem cells empowering tendon regenerative therapies, Int. J. Mol. Sci. 20 (12) (2019) 3002.
[68] N. Sevivas, et al., Mesenchymal stem cell secretome improves tendon cell viability in vitro and tendon-bone healing in vivo when a tissue engineering strategy is used in a rat model of chronic massive rotator cuff tear, Am. J. Sports Med. 46 (2) (2018) 449–459.

[69] The use of cocultured mesenchymal stem cells with tendon-derived stem cells as a better cell source for tendon repair, Tissue Eng. 22 (19–20) (2016) 1229–1240.
[70] E.C. Ekwueme, et al., Cross-talk between human tenocytes and bone marrow stromal cells potentiates extracellular matrix remodeling in vitro, J. Cell. Biochem. 117 (3) (2016) 684–693.
[71] H. Chen, et al., Chemical conjugation of evans blue derivative: a strategy to develop long-acting therapeutics through albumin binding, Theranostics 6 (2) (2016) 243.
[72] Y. Qi, et al., A brush-polymer/exendin-4 conjugate reduces blood glucose levels for up to five days and eliminates poly (ethylene glycol) antigenicity, Nat. biomed. eng. 1 (1) (2016) 1–12.
[73] O. Yanay, et al., Effects of exendin-4, a glucagon like peptide-1 receptor agonist, on neutrophil count and inflammatory cytokines in a rat model of endotoxemia, J. Inflamm. Res. 8 (2015) 129.
[74] L. He, et al., Anti-inflammatory effects of exendin-4, a glucagon-like peptide-1 analog, on human peripheral lymphocytes in patients with type 2 diabetes, J. diabet. investig. 4 (4) (2013) 382–392.
[75] S.S. Iyer, M. Rojas, Anti-inflammatory effects of mesenchymal stem cells: novel concept for future therapies, Expet Opin. Biol. Ther. 8 (5) (2008) 569–581.
[76] B.R. Freedman, et al., Nonsurgical treatment and early return to activity leads to improved Achilles tendon fatigue mechanics and functional outcomes during early healing in an animal model, J. Orthop. Res. 34 (12) (2016) 2172–2180.
[77] J.A. Zellers, et al., Tendon morphology and mechanical properties assessed by ultrasound show change early in recovery and potential prognostic ability for 6-month outcomes, Knee Surg. Sports Traumatol. Arthrosc. 27 (9) (2019) 2831–2839.
[78] T. Andersson, et al., Low-level mechanical stimulation is sufficient to improve tendon healing in rats, J. Appl. Physiol. 113 (9) (2012) 1398–1402.
[79] T. Andersson, P. Eliasson, P. Aspenberg, Tissue memory in healing tendons: short loading episodes stimulate healing, J. Appl. Physiol. 107 (2) (2009) 417–421.
[80] E. Bianchi, et al., Innovative strategies in tendon tissue engineering, Pharmaceutics 13 (1) (2021) 89.
[81] S.E. Udeabor, et al., Characterization of the cellular reaction to a collagen-based matrix: an in vivo histological and histomorphometrical analysis, Materials 13 (12) (2020) 2730.
[82] M. Barbeck, et al., Heterogeneity of biomaterial-induced multinucleated giant cells: possible importance for the regeneration process? J. Biomed. Mater. Res. 104 (2) (2016) 413–418.
[83] R.J. Miron, et al., Giant cells around bone biomaterials: osteoclasts or multi-nucleated giant cells? Acta Biomater. 46 (2016) 15–28.
[84] M. Barbeck, et al., Induction of multinucleated giant cells in response to small sized bovine bone substitute (Bio-Oss™) results in an enhanced early implantation bed vascularization, Ann. maxillof. surg. 4 (2) (2014) 150.
[85] C. Jeong, et al., Exploring the in vivo anti-inflammatory actions of simvastatin-loaded porous microspheres on inflamed tenocytes in a collagenase-induced animal model of achilles tendinitis, Int. J. Mol. Sci. 19 (3) (2018) 820.
[86] P. Sharma, N. Maffulli, Basic biology of tendon injury and healing, Surgeon 3 (5) (2005) 309–316.
[87] L. Ameye, et al., Abnormal collagen fibrils in tendons of biglycan/fibromodulin-deficient mice lead to gait impairment, ectopic ossification, and osteoarthritis, Faseb. J. 16 (7) (2002) 673–680.
[88] K.-i. Matsumoto, et al., The distribution of tenascin-X is distinct and often reciprocal to that of tenascin-C, J. Cell Biol. 125 (2) (1994) 483–493.
[89] F. Elefteriou, et al., Characterization of the bovine tenascin-X, J. Biol. Chem. 272 (36) (1997) 22866–22874.
[90] D. Egging, et al., Wound healing in tenascin-X deficient mice suggests that tenascin-X is involved in matrix maturation rather than matrix deposition, Connect. Tissue Res. 48 (2) (2007) 93–98.
[91] U. Valcourt, et al., Tenascin-X: beyond the architectural function, Cell Adhes. Migrat. 9 (1–2) (2015) 154–165.
[92] C.N. Manning, et al., The early inflammatory response after flexor tendon healing: a gene expression and histological analysis, J. Orthop. Res. 32 (5) (2014) 645–652.
[93] P. Eliasson, T. Andersson, P. Aspenberg, Rat Achilles tendon healing: mechanical loading and gene expression, J. Appl. Physiol. 107 (2) (2009) 399–407.
[94] E. Chisari, et al., Tendon healing is adversely affected by low-grade inflammation, J. Orthop. Surg. Res. 16 (1) (2021) 1–9.
[95] F. Klatte-Schulz, et al., Different Achilles tendon pathologies show distinct histological and molecular characteristics, Int. J. Mol. Sci. 19 (2) (2018) 404.
[96] E. Aktas, et al., Immune modulation with primed mesenchymal stem cells delivered via biodegradable scaffold to repair an Achilles tendon segmental defect, J. Orthop. Res. 35 (2) (2017) 269–280.
[97] H. Asahara, M. Inui, M.K. Lotz, Tendons and ligaments: connecting developmental biology to musculoskeletal disease pathogenesis, J. Bone Miner. Res. 32 (9) (2017) 1773–1782.
[98] S.J. Loder, et al., Characterizing the circulating cell populations in traumatic heterotopic ossification, Am. J. Pathol. 188 (11) (2018) 2464–2473.
[99] S.P. Magnusson, et al., Heterotopic ossification after an Achilles tendon rupture cannot be prevented by early functional rehabilitation: a cohort study, Clin. Orthop. Relat. Res. 478 (5) (2020) 1101.
[100] N. Maffulli, et al., Chondral metaplasia in calcific insertional tendinopathy of the Achilles tendon, Clin. J. Sport Med. 16 (4) (2006) 329–334.
[101] S.-C. Fu, K.-M. Chan, C.G. Rolf, Increased deposition of sulfated glycosaminoglycans in human patellar tendinopathy, Clin. J. Sport Med. 17 (2) (2007) 129–134.
[102] P.P.-y. Lui, et al., Chondrocyte phenotype and ectopic ossification in collagenase-induced tendon degeneration, J. Histochem. Cytochem. 57 (2) (2009) 91–100.
[103] L. Lin, et al., Heterotopic ossification induced by Achilles tenotomy via endochondral bone formation: expression of bone and cartilage related genes, Bone 46 (2) (2010) 425–431.
[104] F. Oliva, et al., Combined ascorbic acid and T3 produce better healing compared to bone marrow mesenchymal stem cells in an Achilles tendon injury rat model: a proof of concept study, J. Orthop. Surg. Res. 14 (1) (2019) 1–10.
[105] M. Schneider, et al., Rescue plan for Achilles: therapeutics steering the fate and functions of stem cells in tendon wound healing, Adv. Drug Deliv. Rev. 129 (2018) 352–375.
[106] J.-I. Liang, et al., Video-based gait analysis for functional evaluation of healing achilles tendon in rats, Ann. Biomed. Eng. 40 (12) (2012) 2532–2540.